Palaeogeography, Palaeoclimatology, Palaeoecology 675 (2025) 113022

Contents lists available at ScienceDirect

Palaeogeography, Palaeoclimatology, Palaeoecology

journal homepage: www.elsevier.com/locate/palaeo

Ten years of *Tridacna* sclerochemistry at up to daily resolution from a controlled aquarium environment – Records of habitat change, induced seasonality and growth variability

Max Fursman [a,b,*], Viola Warter [c], Max Janse [d], Willem Renema [e,f], Christoph Spötl [g], Iris Arndt [a,b], David Evans [a,b,h], Wolfgang Müller [a,b,*]

[a] Institute of Geosciences, Goethe University Frankfurt, Frankfurt am Main, Germany
[b] Frankfurt Isotope and Element Research Center (FIERCE), Goethe University Frankfurt, Frankfurt am Main, Germany
[c] Department of Earth Sciences, Royal Holloway University of London, London, UK
[d] Royal Burgers' Zoo, Arnhem, the Netherlands
[e] Marine Biodiversity group, Naturalis Biodiversity Center, Leiden, the Netherlands
[f] Institute for Biodiversity and Ecosystem Dynamics (IBED), University of Amsterdam, Amsterdam, the Netherlands
[g] Institute of Geology, University of Innsbruck, Innsbruck, Austria
[h] School of Ocean and Earth Science, University of Southampton, Southampton, UK

ARTICLE INFO

Editor: M Elliot

Keywords:
Daily cycle
LA-ICPMS
Culturing
Giant clam
Stable isotopes
Growth rate
Biophysiological stressor

ABSTRACT

Giant clams such as *Tridacna* sp., with their rapid shell accretion (mm-cm/year), decade-long lifespans and aragonitic shells, are invaluable (palaeo)environmental archives, potentially providing information at (sub-) seasonal timescales. Royal Burgers' Zoo aquarium in Arnhem, The Netherlands, opened a live coral reef eco-display in 2000 and introduced *T. squamosa* from Vietnam in 2001. One specimen (TS2) that died in 2011 facilitated a decade-long comparison of carefully monitored aquarium conditions with *Tridacna* sclerochemistry and growth, whose results we present herein. Spatially resolved El/Ca ratios by LA-ICPMS (at up to daily resolution) as well as micromilled $\delta^{13}C$ and $\delta^{18}O$ data were transferred onto a sclerochronological framework at a daily resolution, which enabled the detailed correlation of aquarium parameters with sclerochemistry. We show that environmental stresses such as transportation, introduction to a new aquarium environment, shifts in water change regimes and artificial seasonality from 2009 onwards have severe impacts on the organism's growth and sclerochemistry, and are particularly manifest in this sample in increased Mg/Ca and Sr/Ca ratios. Growth rates were reduced from ~20 to ~7 μm/day during transportation into the aquarium, and from ~10 to ~2 μm/day during shifts in water change regimes in the aquarium. A disruption of daily El/Ca cyclicity was marked during transportation-induced stress, but within three weeks of introduction the organism acclimatised to the aquarium and returned to natural growth rates and cyclicity. Three years of induced temperature seasonality (25.0–26.5 °C) most notably affected Na/Ca, while the resulting expected $\delta^{18}O$ variability was not resolvable due to TS2's strongly decreased growth rate coupled with our large drill-step size for sampling. Despite a transient spike in aquarium [NO_3^-] from ~0.02 to 2.4 mg/L, caused by accidental over-fertilisation, no stress effect was apparent in the organism's sclerochemistry or growth rate. Changes in the water-exchange regime appear to have far more sclerochemical impact, as these are reflected in the overall $\delta^{18}O$, Ba/Ca and associated growth rates. The detailed decade-long *Tridacna* record shows that even systems with comparatively little environmental variability can produce large degrees of shell heterogeneity, and also highlights the importance of establishing a detailed (counted) chronology for sclerochemical interpretations.

1. Introduction

Geochemical proxies from various natural archives such as corals, foraminifera, or molluscs are widely used tools for reconstructing past environmental conditions. They provide information about long-term climate variability and help to establish a historical context for current

* Corresponding authors at: Institute of Geosciences, Goethe University Frankfurt, Frankfurt am Main, Germany.
E-mail addresses: fursman@em.uni-frankfurt.de (M. Fursman), w.muller@em.uni-frankfurt.de (W. Müller).

https://doi.org/10.1016/j.palaeo.2025.113022
Received 3 July 2024; Received in revised form 3 April 2025; Accepted 12 May 2025
Available online 17 May 2025
0031-0182/© 2025 The Authors. Published by Elsevier B.V. This is an open access article under the CC BY license (http://creativecommons.org/licenses/by/4.0/).

and future climate trends (Chauvaud et al., 2005; Elliot et al., 2009; Gröcke and Gillikin, 2008; Jones et al., 1989; Prendergast et al., 2017; Schöne and Fiebig, 2009; Vieten and Hernandez, 2021; Weidman et al., 1994). Shell geochemical compositions, including isotopic and (trace) elemental data of well-preserved parts, are useful proxies that reflect - through the lens of biomineralisation - past seawater conditions. Thus, growth-banded archives provide information on events ranging from hourly and daily to centennial and millennial scales (Freitas et al., 2005; Johnson et al., 2009; Jones and Quitmyer, 1996; Jones et al., 2005; Sano et al., 2021; Surge and Walker, 2006). Specifically, proxies such as $\delta^{18}O$, $\delta^{13}C$ or element/Calcium (El/Ca) ratios are suitable for inferring information about parameters such as sea-surface temperature (SST) (Alibert and McCulloch, 1997; Ayling et al., 2015; Lopes Dos Santos et al., 2013; Schöne et al., 2002), salinity (Klein et al., 1996) and nutrient availability (Carré et al., 2006; Elliot et al., 2009; Meibom et al., 2007; Purton et al., 1999; Schöne and Gillikin, 2013; Yan et al., 2014).

Among the organisms used in palaeoclimate studies, giant clams of the *Tridacninae* subfamily are a particularly attractive archive due to a variety of life-history traits. Their growth rate is characterised by rapid shell accretion of mm/yr – cm/yr, leaving macroscopically visible seasonal banding at mm scales to microscopically visible daily banding at μm scales (Arndt et al., 2023; Bonham, 1965; Faylona et al., 2011; Immenhauser et al., 2016; Sano et al., 2012; Warter et al., 2018). *Tridacna* are characterised by their longevity, with lifespans of several decades (Comfort, 1957; Rosewater, 1965; Selin and Latypov, 2011; Ungvari et al., 2013). They also have photosymbionts and therefore record near-surface conditions (Ishikura et al., 1997; Jantzen et al., 2008; Lucas, 1994).

Previous studies have shown that *Tridacna* precipitate their shells close to oxygen isotopic equilibrium, thus providing the possibility to quantify past changes in SST and/or $\delta^{18}O_{seawater}$ (Aharon, 1983; Aharon and Chappell, 1986; Arndt et al., 2025; Watanabe and Oba, 1999; Welsh et al., 2011). Depending on shell growth rates, spatially-resolved sampling of these shells on a cm – mm – μm scale can yield environmental information on decadal to sub-daily timescales: short-lived species can also record seasonality and weather extremes, while long-lived species can record climatic oscillations across decades (Gannon et al., 2017; Pätzold et al., 1991; Prendergast et al., 2017; Warter et al., 2018; Welsh et al., 2011). The dense aragonitic shell of *Tridacna* also provides an advantage in palaeoclimate studies, as the fine-scale layering of the shell makes it relatively impervious, limiting diagenetic alteration including dissolution, recrystallisation and precipitation of secondary calcite. In contrast to their more thin-walled and perforated coral counterparts, *Tridacna* often show better shell preservation with a largely pristine preservation being relatively common, even in samples that are millions of years old (Aharon, 1991; Arndt et al., 2023; Batenburg et al., 2011; Harzhauser et al., 2008; Schöne et al., 2002; Warter et al., 2015).

It is important to recognise that the interpretation of sclerochemical data in terms of environmental parameters such as temperature, pH, nutrient concentrations or light availability relies on developing an understanding of the processes that control the incorporation of geochemical proxies into the shell material, i.e. the existence of a transfer function or proxy calibration (Henderson, 2002; McClelland et al., 2021; Müller and Fietzke, 2016; Sanyal et al., 2000). Calibration studies ideally utilize samples grown in carefully controlled environments in order to establish the relationship between environmental variables and a (bio)geochemical proxy (Goodwin et al., 2001, 2003; Gornitz, 2009; Jansen et al., 2007; Owen et al., 2016; Pérez-Huerta et al., 2013; Schöne et al., 2005). While such studies have been carried out based on short-term culturing experiments (Liu et al., 2020; Mies et al., 2012; Warter et al., 2018), there is a need for long-term culturing experiments spanning several years. Such studies will serve to examine the factors that affect the incorporation of chemical tracers into the shell on seasonal to multi-annual time scales, and to avoid the possible bias that may arise via the measurement of shell material deposited while the organism is still undergoing acclimatisation. Given the typical lifespan of *Tridacna* species of several decades (Selin and Latypov, 2011; Ungvari et al., 2013), culturing experiments that elucidate how seasonal changes affect proxies across several years are possible. However, setting up and monitoring of such a long-term culturing experiment is costly and time-consuming.

Here, we alternatively present data from an indirect culturing experiment that was set up by Royal Burgers' Zoo Aquarium, Arnhem, The Netherlands. In April 2000 the zoo opened “Burgers' Ocean”, a 750,000 l tank containing a live coral reef in order to showcase several marine ecosystems (Janse et al., 2008), for which high-quality monitoring data are available. As part of the exhibit specimens of different species were relocated from natural environments in Vietnam, including several *Tridacna squamosa* specimens.

In this study, we use the opportunity provided by this exhibit to compare results from sclerochemical proxies against environmental parameters during the long-term growth of one of these *T. squamosa* clams, focusing on the factors that influence growth and the incorporation of geochemical proxies into the shell. Given the slightly greater than ten-year study period, this provides a valuable long-term dataset that helps to assess the reliability of palaeoenvironmental reconstructions based on giant clams.

2. Materials and methods

2.1. Sample background and preparation

The *T. squamosa* sample used in this study (henceforth referred to as ‘TS2’, registered in the Zoological Information System ZIMS as ARNHEM/610921) originated from the coast of Vietnam, where it was live-captured and transported to Burgers' Zoo and placed into the Burgers' Ocean living coral reef tank. Details of the set-up of the exhibit can be found in Janse et al. (2008). The exact conditions and timing of the specimen transfer are not known, as no registration exists for the specimen, but according to aquarium records it underwent no quarantine period upon arrival and was introduced to the aquarium in October 2001, where it lived until its death in December 2011. A previous study (Batenburg et al., 2011) presented results of another *T. squamosa* specimen introduced into Burgers' Ocean coral tank, which lived there for only ~3 years.

As TS2 was kept in a controlled and monitored artificial reef environment for >10 years, it thus provides a decade-long record of how changing conditions in the tank affected its growth and sclerochemistry. Artificial seasonality was introduced to the Burgers' Ocean in 2009, with the temperature being regulated throughout the year between 25 and 26.5 °C, well within the natural tolerance of *Tridacna* species (Eckman et al., 2019; Estacion and Braley, 1988; Gomez and Belda, 1988; Heslinga et al., 1984; Trinidad-Roa, 1988), to better reflect the natural conditions of the coral environment (Janse et al., 2008). Temperature, salinity and pH of the aquarium was monitored regularly (Janse et al., 2008). Furthermore, the key seawater trace elements were measured every four to six months for the first few years using Inductively Coupled Plasma Mass Spectrometry (ICPMS) (Janse et al., 2008). We therefore have detailed environmental records for comparison with sclerochemical changes. In January 2007, sodium nitrate was accidentally added to the tank instead of sodium carbonate, which led to a nitrate concentration spike (Janse et al., 2008). After 200 days the nitrate concentration returned to typical pre-spike values. Some corals died and most corals stopped growing as a result, but the *Tridacna* specimen TS2 survived intact, at least physically, for another four years. For the purpose of this study this event is referred to as the ‘nitrate spike’.

TS2 was cleaned and cut from the umbo to the ventral margin along the maximum growth axis, before a smaller section of shell was cut in order that it could be place into the sample holder of the laser ablation instrument utilised here (Müller et al., 2009) for subsequent analysis (henceforth referred to as ‘the slab’) (Figs. 1, 2). From this thick section,

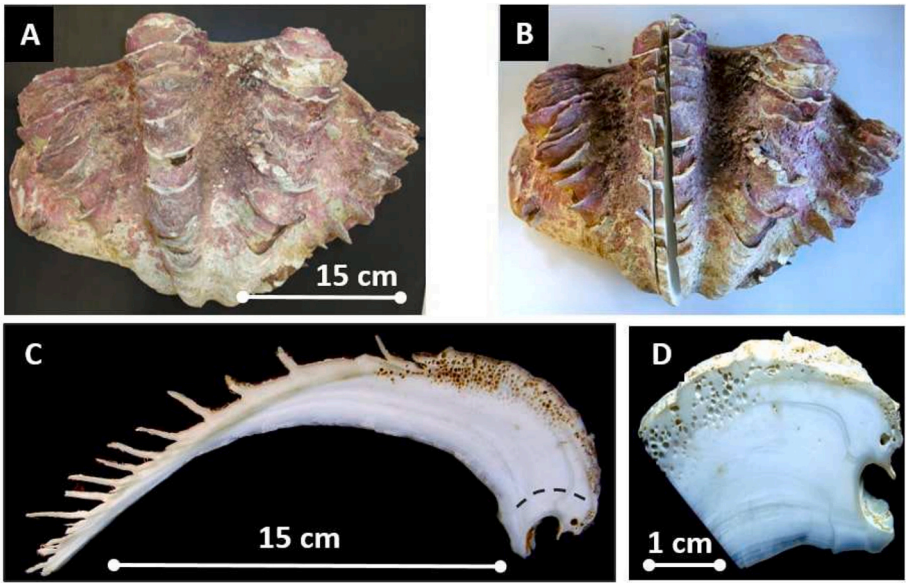

Fig. 1. (A) Intact *T. squamosa* sample from Burgers' Zoo Aquarium. (B) *T. squamosa* showing cut section along the growth axis for analysis. (C) Cross section view of the cut portion of shell; dotted lines indicate the growth axis. (D) Portion of shell removed for chemical analysis and thin sections preparations.

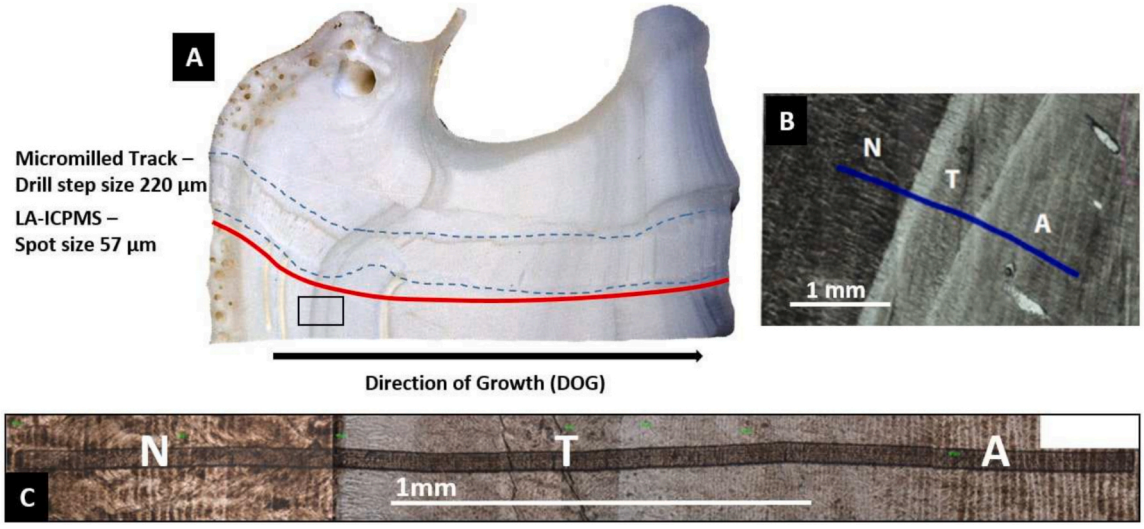

Fig. 2. (A) TS2 slab sampled for stable isotope analysis and on which the lower-resolution laser ablation track was placed. The position of the micromilled track is indicated by the two dotted blue lines; sampling was carried out using a milling increment of 220 µm. Low-spatial resolution LA-ICPMS analysis across the growth axis of the shell followed the red track indicated, using a spot size of 57 µm. (B) Transmitted light image of the thin section indicated by the black square in A, showing the analysis track by the laser. 'N' indicates the region of shell understood to have grown in nature, 'T' the portion of shell grown during transportation and 'A' the portion understood to have grown in the aquarium. (C) Close-up of the ablated track, in transmitted light, with clearly defined growth banding in nature and, after an acclimatisation period, in the aquarium habitats. (For interpretation of the references to colour in this figure legend, the reader is referred to the web version of this article.)

a thin section of 30 µm thickness was prepared using a surface grinder and both sections were polished with a diamond suspension. The thin section was used for both imaging and Laser Ablation-ICPMS (LA-ICPMS) analysis at a high-spatial resolution (4 × 50 µm on-sample spot size), while the thick section was used for micromilling and initial lower spatial-resolution LA-ICPMS analysis (57 µm).

2.2. Laser ablation-inductively coupled plasma mass spectrometry (LA-ICPMS) analysis

Spatially-resolved trace elemental analysis was conducted using the LA-ICPMS system at Royal Holloway University of London (RHUL) (Müller et al., 2009), featuring the prototype RESOlution M-50 laser-ablation system (193 nm) with a Laurin Technic M-50 two-volume LA cell connected to an Agilent 7500ce ICPMS. Analytical procedures followed Warter et al. (2015) and Warter et al. (2018) and are summarised in Table 1. Instrument tuning was performed using the standard reference materials NIST SRM610 and NIST SRM612 (Jochum et al., 2011) to ensure optimal sensitivity (maximum signal to background ratio) while maintaining robust plasma conditions.

Prior to analysis, the slab and the thin section were ultrasonically cleaned using deionised water and ethanol. Two profiles were measured, with a continuous lower-resolution path placed on the slab and a higher resolution path was placed on the thin section. For the slab, a spot-size of 57 µm and a scan speed of 30 µm/s were used to obtain elemental data along a continuous track across the entire life history of the organism

Table 1
LA-ICPMS operational parameters. Two profiles were measured on the sample at differing spatial resolutions, termed 'slab' and 'thin section', see text for details.

ICPMS parameters	Agilent 7500ce
RF power	1140–1320 W (optimised daily)
Carrier gas flow (Ar)	0.53–0.67 l/min (optimised daily)
Sampler, skimmer cones	Ni
Extraction lenses	CE
Tuning parameters	$^{232}Th/^{238}U > 95$ %; $^{248}ThO/^{232}Th < 0.5$ %
Laser ablation system	RESOlution M-50
Laser spot-size	57 μm ('slabs') and 4 × 50 μm ('thin section')
Scan Speed	30 μm/s ('slabs') and 1.5 μm/s ('thin section')
Laser Repetition Rate	15 Hz
He gas flow	850 ml/min
H gas flow	8.5 ml/min (added downstream of LA cell)
Laser Fluence	4.5 J/cm^2

(preceded by a preablated path of 74 μm spot-size), perpendicular to growth banding along the growth axis (Fig. 2). Monitored analytes were: ^{11}B, ^{23}Na, ^{24}Mg, ^{25}Mg, ^{27}Al, ^{31}P, ^{43}Ca, ^{55}Mn, ^{65}Cu, ^{66}Zn, ^{85}Rb, ^{88}Sr, ^{89}Y, ^{95}Mo, ^{97}Mo, ^{111}Cd, ^{138}Ba, ^{139}La, ^{140}Ce, ^{208}Pb and ^{238}U. Only results of ^{11}B ^{23}Na, ^{24}Mg, ^{38}Sr, and ^{138}Ba will be discussed as other trace elements showed little variability or were below the Limit of Detection (LOD) (Supplementary Fig. S1).

To obtain elemental data at a very high spatial resolution while maintaining useful sensitivity, a rotating rectangular aperture was used to obtain a spot-size of 4 × 50 μm with a scan speed of 1.5 μm/s (Warter et al., 2018). The long axis aperture slit was aligned with the visible (daily) growth bands. The analysis traced a path across regions of the shell that had previously been determined to be the periods of TS2's life history immediately prior to, during, and following transport from Vietnam to The Netherlands (Fig. 2). The measurements were performed in continuous profiling mode and a total sweep time of 370 ms which was kept short by analysising six elements (m/z ^{11}B, ^{24}Mg, ^{43}Ca, ^{88}Sr, ^{89}Y and ^{138}Ba). A pre-ablation cleaning using the same rectangular spot preceded data acquisition.

LA-ICPMS data reduction followed Longerich et al. (1996) and was performed using Iolite v4.8 software (Paton et al., 2011). Internal standardisation was performed using ^{43}Ca while external standardisation utilised NIST SRM612, with the accuracy on analyses assessed via the MPI-DING glasses GOR128, GOR132 and KL2-G (Jochum et al., 2011), treated as unknowns and periodically analysed in exactly the same manner as the samples. The reported NIST SRM612 values of Jochum et al. (2011) were used with the exception of Mg, for which we followed the recommendation of Evans and Müller (2018). The resulting accuracies and the precisions are shown in Table 2.

2.3. Micromilling

Powdered aragonite samples were obtained from the thick section of TS2 using a semiautomated New Wave micromill at RHUL. Single grooves with a length of 2 mm, a depth of 360 μm and a width of 220 μm were milled parallel to existing growth bands in continuous mode using a 300 μm drill bit. Samples were analysed for carbon and oxygen isotope ratios using a continuous-flow isotope ratio mass spectrometer (IRMS) at the University of Innsbruck (Spötl and Vennemann, 2003).

External precision (1 SD) of an international standard (NBS-19) and an in-house standard were 0.08 ‰ for $\delta^{18}O$ and 0.07 ‰ for $\delta^{13}C$. Sample data are expressed in conventional delta notation (per mil) relative to VPDB.

2.4. Imaging/reflected-light darkfield illumination photography (RLDI)

The macroscopically visible distinct banding (Fig. 2) was microscopically imaged using the thin section to identify characteristically alternating light-dark bands that are typical of daily growth increments.

Previous work has shown that each light-dark band couple represents a single year of growth in the organism's life (Aharon, 1991; Batenburg et al., 2011; Elliot et al., 2009; Warter et al., 2015). Daily growth bands within these annual bands have previously been reported (Liu et al., 2022; Sano et al., 2012; Warter et al., 2015; Watanabe and Oba, 1999; Watanabe et al., 2004; Zhao et al., 2023) and are similarly identifiable in the sample utilised here.

The microscopic shell structure was imaged with a Keyence VHX-6000 microscope using a polished thin section with full ring incident light at the Institute of Geosciences, Goethe University Frankfurt, Frankfurt am Main (GUF). Overview images were obtained to assess the banding present at 20× magnification, with successive images using 400× to 2000× magnification to obtain a high-resolution image of the entire shell. Some regions of the shell, especially within the last ~5 mm of growth, showed extensive dark banding, such that daily growth increments could not be discerned with certainty. Therefore, the thin section was re-imaged using reflected-light darkfield illumination (RLDI) with a Canon 5D Mark II with 25 and 50 mm loupe lenses that provided better resolved images of daily growth increments (Supplementary Fig. 2).

All microscopic images were viewed using the image edition software GIMP 2.10 to mark off visible daily banding and to obtain a manually counted chronology of the shell.

2.5. Aquarium seawater and monitoring

Artificial seawater used in the aquarium was produced from fresh water that initially underwent reverse osmosis. The same water supplier

Table 2
Accuracy and precision determined using the standard reference materials GOR128, GOR132 and KL2-G, compared to their reference values (GeoReM preferred values; Jochum et al., 2006).

El	Standard	Measured mean (μg/g) ± 2SD	Reference value (μg/g) ± 2SD	Accuracy (%)	Precision (% 2 RSD)
B	GOR128	23.4 ± 2.7	23.1 ± 1.8	0.99	11.5
	GOR132	19.1 ± 1.1	17.2 ± 1.0	10.87	5.6
	KL2-G	3.0 ± 1.0	2.7 ± 0.3	10.48	34.6
Na	GOR128	3985 ± 120	4275 ± 197	−6.77	3.0
	GOR132	5533 ± 271	6157 ± 30	−10.15	4.9
	KL2-G	$1.496e^4 \pm 0.067E^4$	$1.743e^4 \pm 0.059e^4$	−14.20	4.5
Mg	GOR128	$1.571e^5 \pm 0.074e^4$	$1.550e^5 \pm 0.052e^4$	1.35	4.7
	GOR132	$1.339e^5 \pm 0.0625e^5$	$1.35e^5 \pm 0.01e^5$	−0.86	4.7
	KL2-G	$4.358e^4 \pm 0.15e^4$	$4.427e^4 \pm 0.054e^4$	−1.60	3.4
Sr	GOR128	30.3 ± 1.7	29.7 ± 1.8	1.89	5.8
	GOR132	15.1 ± 0.9	15.3 ± 1.6	−1.65	6.1
	KL2-G	354.2 ± 14.2	356 ± 8.0	−0.50	4.0
Ba	GOR128	1.06 ± 0.03	1.07 ± 0.16	−0.87	2.6
	GOR132	0.99 ± 0.34	0.82 ± 0.06	21.88	34.0
	KL2-G	116.4 ± 4.69	123 ± 5	−5.38	4.0

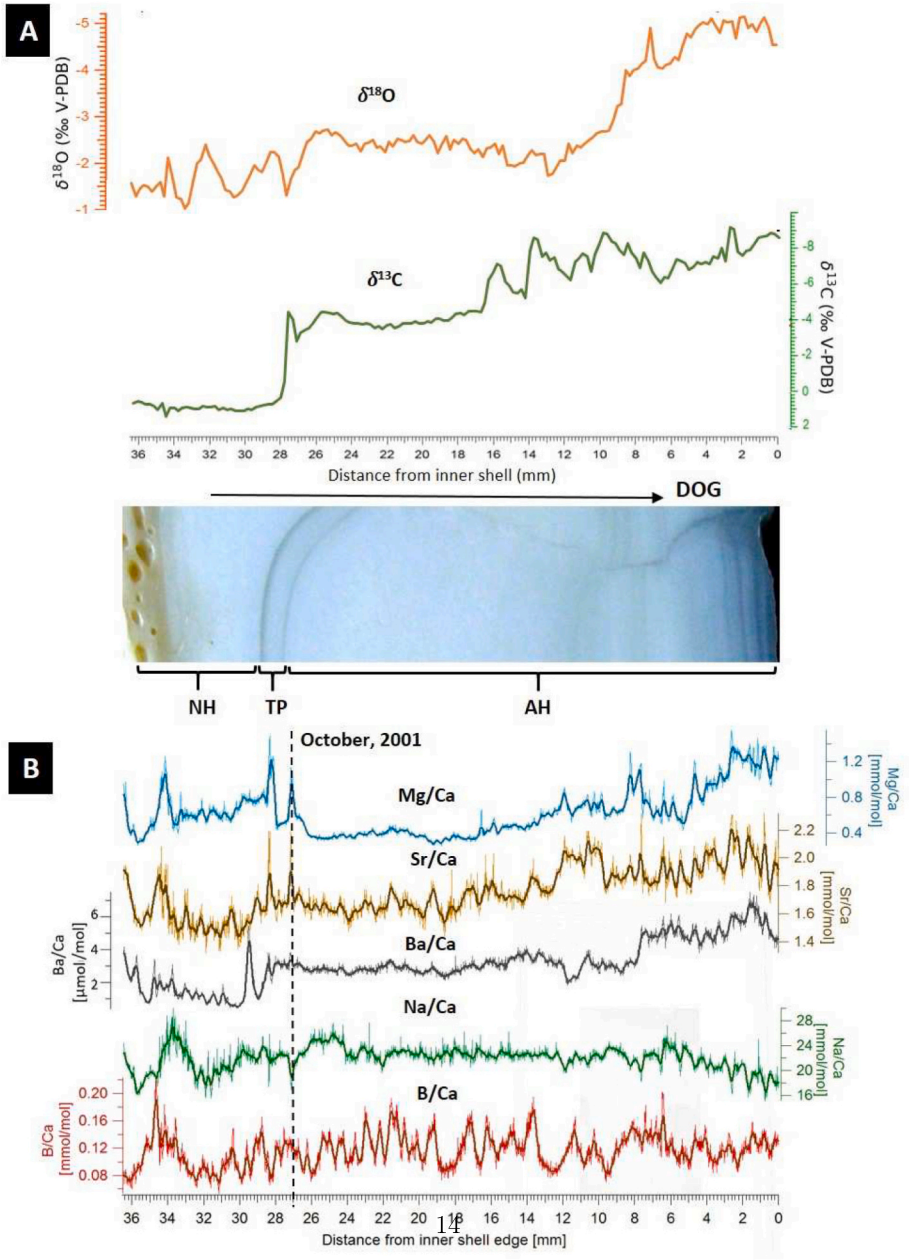

Fig. 3. (A) Spatially-resolved $\delta^{13}C$ and $\delta^{18}O$ data of TS2 (note reversed x axis). Direction of growth (DOG) from left to right, 36–28 mm represents the growth period in the natural environment, while 27–0 mm occurred in the aquarium. (B) Lower-resolution LA-ICPMS El/Ca profile from TS2 ('slab' data, see text for details). The dashed line shows the position of October 2001, when TS2 was introduced to the aquarium setting.

was used throughout. Burgers' Zoo Aquarium monitored the temperature, salinity, and pH of the live coral tank using WTW TetraCon 700 and WTW Sensolyt SEA probes with a WTW pH 296. Nutrients were measured once a month using HACH spectrometer (Method 8192 for nitrate and Method 8048 for ortho-phosphate), and major trace elements were measured every four to six months using ICPMS. Technical setup and details of monitoring are listed in Janse et al. (2008). See Table S1 for details.

3. Results

All results are displayed in Figs. 3–5. Aquarium monitoring, stable isotope and LA-ICPMS data are given in Supplementary Tables S1–6 in the supplementary datasets 1 and 2.

3.1. Stable isotope data

Profiles of the oxygen and carbon stable isotopic compositions ($\delta^{13}C$ and $\delta^{18}O$) of TS2 are shown in Fig. 3A. Both $\delta^{13}C$ and $\delta^{18}O$ profiles display a near continuous decrease in their respective values across TS2's life.

In order to assess the relative timing of periods of growth in natural conditions in Vietnam and those in the aquarium setting, the results of the stable isotope analyses of TS2 were compared to the results obtained by Batenburg et al. (2011). This study was on another sample of *T. squamosa* from Burgers' Zoo that was similarly obtained from the Vietnam coast and introduced to the aquarium at the same time as TS2 but which died within three years of transfer. Those authors noted that C showed a strong shift to more negative $\delta^{13}C$ values (~+1 to −4 ‰) upon what was calculated to be the transition from natural to aquarium conditions, accompanied by a distinct transitional surface. We see a very

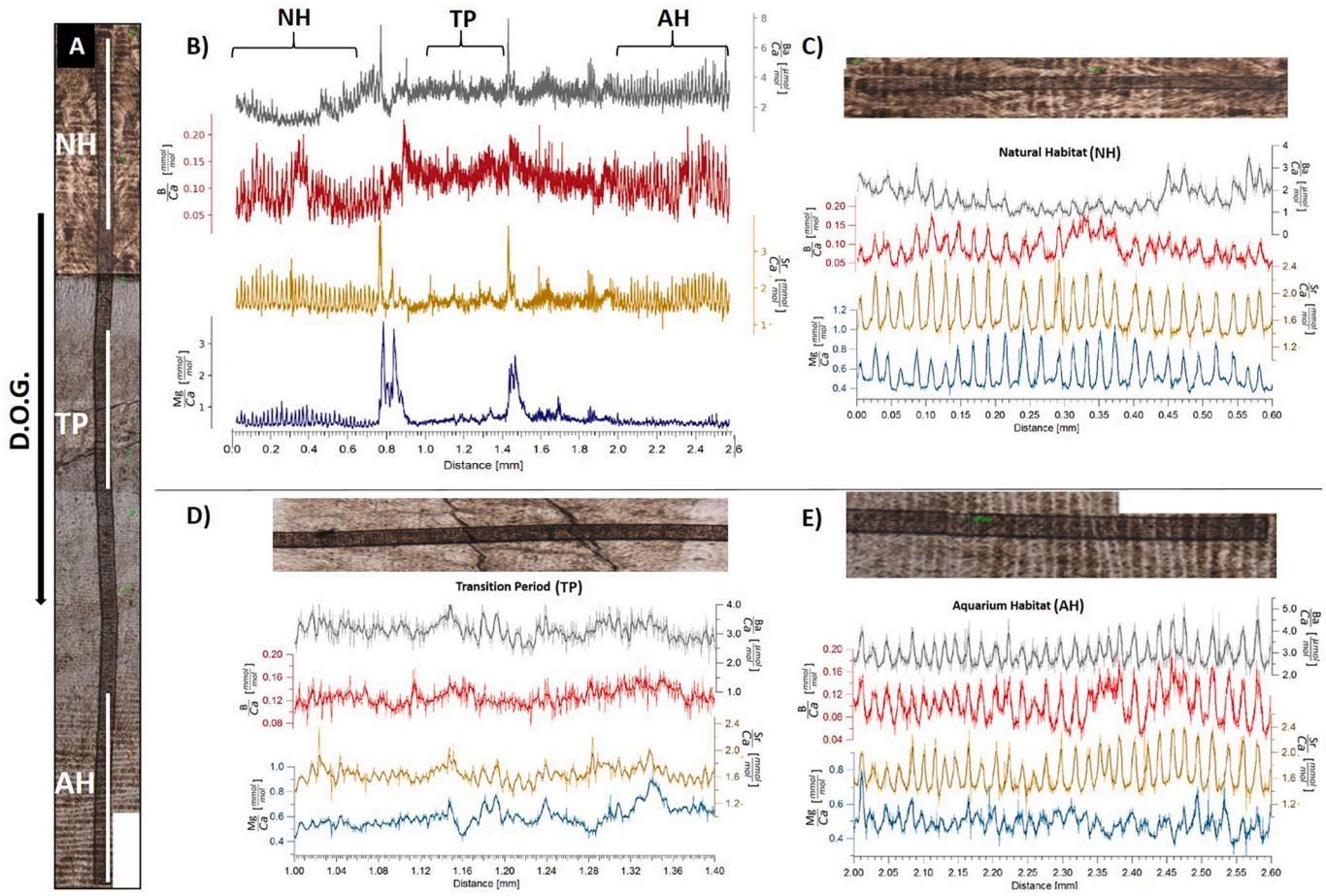

Fig. 4. (A) Shell image montage showing the laser track across the portion of the shell spanning the transition from the natural habitat growth (NH), across the transition period (TP), and the initial aquarium habitat growth period (AH). Portions of the dataset expanded in panel C-E are indicated by white lines adjacent to the laser track. (B) (Sub)daily resolved LA-ICPMS results from across the TP using a rectangular slit of 4 × 50 μm. Brackets at the top indicate sections of analysis magnified in panels C – E, see text for details. (C) Expanded view of shell chemistry during an interval that the organism lived in its NH. (D) Expanded view of the TP. (E) Expanded view of shell chemistry shortly after introduction into the AH.

similar phenomena in TS2, with C shifting from +0.9–1.1 ‰ to −3.5 to −4.2 ‰ at ~28 mm on the shell (Supp. Fig. S3), associated by a clearly visible dark double banding between ~28–27 mm from the inner shell (Fig. 3A). The section of shell between these bands is dubbed the 'transition period' (hereafter referred to as TP), with the preceding section of shell representing the period of life history in Vietnamese coastal waters, hereafter referred to as the 'natural habitat' (NH), and the succeeding section representing the period of life history in the aquarium setting, hereafter referred to as the 'aquarium habitat' (AH).

Shell $\delta^{13}C$ is broadly constant at ~1 ‰ during the NH period and remains constant following the TP at ~-3 ‰ for the first half of AH growth, until ~15 mm. Oscillations between ~-4 to ~-8 ‰ imprint on an overall negative trend over the next ~10 mm of growth, after which there is less variability, although the negative trend continues with values decreasing from ~-6 to ~-8 ‰ in the last ~7 mm of growth.

The oxygen isotope ($\delta^{18}O$) profile is characterised by cyclicity during the NH growth (~36–28 mm), with three main points of variation between ~-1 to ~-2.5 ‰. Following the transition to the AH, the values shift from −1.5 to ~-2.5 ‰, where they remain with some minor variation until ~10 mm, at which point there is a negative trend over the next 8 mm of growth to ~-5 ‰. During the last 5 mm of growth $\delta^{18}O$ remains broadly constant at this value with variations of <~0.5 ‰ until death.

3.2. Spatially-resolved trace elemental data (LA-ICPMS)

3.2.1. 'Low-resolution' whole shell transect

The LA-ICPMS results of TS2 display four distinct areas of variability, namely the portions ~36 to ~28 mm, ~28 to ~27 mm, ~27 to ~12 mm and ~12 to 0 mm, relative to the inner shell surface and thus in direction of growth (Fig. 3). Based on the $\delta^{13}C$ results of the profile the first period of variability is the section of shell that grew naturally off the coast of Vietnam.

The most prominent variation during the first period occurs within the first ~2–4 mm of life history (~36 to ~32 mm from the outer shell edge). The elemental ratios of the LA-ICPMS profile vary from 0.4 to 1.2 mmol/mol (Mg/Ca), 1.6–2.0 mmol/mol (Sr/Ca), 1–4 μmol/mol (Ba/Ca), 16–28 mmol/mol (Na/Ca) and 0.08–0.20 mmol/mol (B/Ca). Given that we focus here on the periods of controlled growth in the AH, and lack detailed in situ monitoring data for the field site, we do not attempt to interpret the cause of this variability.

The TP is bound on either side by sharp peaks in Mg/Ca and Sr/Ca of ~1.2 mmol/mol and ~2 mmol/mol respectively. Na/Ca shows a corresponding drop to ~16 mmol/mol. Ba/Ca is characterised by a shift from ~0.5 μmol/mol in natural conditions to ~3 μmol/mol. B/Ca displays periodic variations between ~0.08–0.14 mmol/mol, a trend that appears to be a continuation of that seen in nature prior to the transition.

The third distinct interval of shell geochemistry, between ~27 – ~12

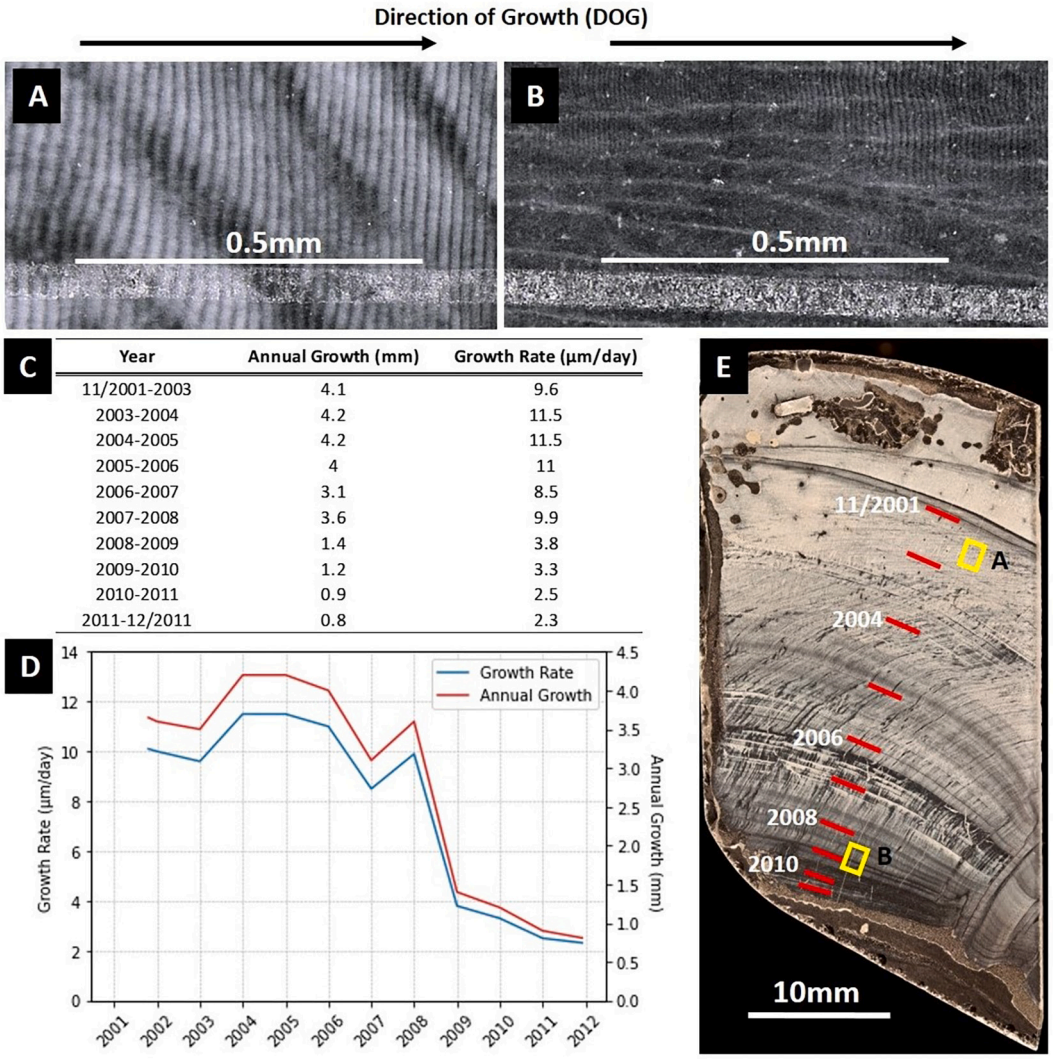

Year	Annual Growth (mm)	Growth Rate (µm/day)
11/2001-2003	4.1	9.6
2003-2004	4.2	11.5
2004-2005	4.2	11.5
2005-2006	4	11
2006-2007	3.1	8.5
2007-2008	3.6	9.9
2008-2009	1.4	3.8
2009-2010	1.2	3.3
2010-2011	0.9	2.5
2011-12/2011	0.8	2.3

Fig. 5. (A) and (B) Micrographs of equal-sized portions of the shell of TS2 from early and late growth domains following introduction into the aquarium. (A) Distinct daily banding of ~26 bands from the first year of growth within the aquarium. (B) Far less well discernible daily banding, corresponding to ~68 bands from a portion of the shell formed several years later. (C, D) Annual growth (mm) and growth rate (µm/day) of TS2 from the date of entry into the aquarium until death. (E) RDLI image of the TS2 thin section. Yellow boxes marked A and B indicate the regions in panels A and B are imaged from. Red lines show the shell chronology (only every second year of growth is labelled).

mm, reflects the time when TS2 was growing in the AH but before seasonality was induced in the aquarium. Overall, this portion of the shell is characterised by relatively low levels of sclerochemical variability compared to the periods before and after. Specifically, this portion is characterised by Mg/Ca, Ba/Ca, and Na/Ca variability between 0.4 and 0.6 mmol/mol, 3.0–3.5 µmol/mol and 22–24 mmol/mol respectively. In contrast, Sr/Ca and especially B/Ca displays variation in the form of clear cyclicity, with repeated variations between 1.6 and 1.9 mmol/mol and 0.09–0.17 mmol/mol respectively.

Between ~12–0 mm there is another marked change in both variability and absolute values compared to the previous sections. A more cyclical nature in Sr/Ca, Ba/Ca, and Na/Ca is visible, with variations between 1.8 and 2.2 mmol/mol, 3–6 µmol/mol and 16–25 mmol/mol respectively. Mg/Ca is characterised by an even greater relative degree of variability and rises to an apparent plateau of variation of ~1.3 mmol/mol, the highest values observed across the entirety of the shell. The final 2–3 mm of shell growth displays a pronounced decrease in Sr/Ca and Ba/Ca, while Na/Ca also displays such a decrease but starting from 6 mm.

3.2.2. *Transition period at daily time resolution*

Across the TP of TS2, a rotating rectangular aperture-slit mask (4 × 50 µm) was used in order to assess how growth conditions of the NH, TP and AH affected El/Ca ratios at (sub)daily resolution. Significant variability for El/Ca ratios (Ba/Ca, B/Ca, Sr/Ca, and Mg/Ca) can be observed within all three distinct sections analysed (Fig. 4). Within the NH and AH sections clear compositional cycles occur, in contrast to the TP which lacks well-defined El/Ca cyclicity with the exception of Sr/Ca, for which cycles with a reduced amplitude are visible. As in the lower-resolution LA data described above, peaks at ~0.8 mm and ~1.5 mm are observed in the Mg/Ca, Sr/Ca and Ba/Ca profiles (~0.5–3.5 mmol/mol, ~1.5–3.5 mmol/mol and ~3–7 mol/mol respectively) at the start and end of the transition. The Mg/Ca peaks heights are greater than those in the lower resolution dataset (~2–3.5 mmol/mol compared to ~1.2 mmol/mol) due to the narrower spot size resulting in less mixing with shell material from other growth periods. Comparing these three distinct sections of life history highlights stark differences in cyclicity between transition and non-transition periods (Fig. 4).

3.2.2.1. Natural habitat. The NH period (Fig. 4C) shows clear oscillations in B/Ca, Sr/Ca, and Mg/Ca ratios of 0.05–0.15 mmol/mol, 1.4–2.2

mmol/mol and 0.4–0.9 mmol/mol respectively. This cyclicity matches the growth banding present, with each of the 27 El/Ca peaks observed in this portion of the shell aligning with a corresponding dark growth band, from which a daily growth rate of ~22 μm/day can be derived. These chemical bands are of similar magnitude throughout this portion of the shell, except in the case of the B/Ca data between 0.3 and 0.4 mm, where there is a period of ~4 days of growth in which the oscillations reduce in amplitude but are still discernible.

Ba/Ca values range between 1 and 3.5 μmol/mol, with less well-defined oscillations compared with the other El/Ca ratios. While there is a correlation with the banding and peaks of other elements, an increase in amplitude occurs within the last week of shell growth included in this segment, with a change from 1.0 to 1.5 μmol/mol to 1.5–3 mol/mol.

3.2.2.2. Transition period. The TP (Fig. 4D) is the section during which TS2 was undergoing transportation (0.8–1.5 mm on the track in Fig. 4). The El/Ca ratios of this period show little to no daily cyclicity, nor can growth bands be accurately determined. Ba/Ca and B/Ca ratio ranges are reduced compared to natural conditions, being 2.5–4 μmol/mol and 0.10–0.15 mmol/mol respectively. Sr/Ca and Mg/Ca ratios are characterised by less reduction in heterogeneity, with ranges of 1.4–1.8 mmol/mol and 0.4–0.8 mmol/mol respectively, but the contrast is stark regarding the lack of oscillatory compositional change compared with the natural growth. Thus, the growth rate during this portion of the organism's life is difficult to determine. Counting of the growth bands that can be discerned results in an estimate of ~60 days, which approximately matches the number of reduced amplitude Sr/Ca bands (~50 ± 5) and yields a greatly reduced growth rate of ~7 μm/day.

3.2.2.3. Aquarium habitat. El/Ca (Fig. 4E) ratios in the AH portion of the shell show a return to clearly defined oscillations, between 2.5 and 4.5 μmol/mol (Ba/Ca), 0.06–0.16 mmol/mol (B/Ca), 1.4–2.2 mmol/mol (Sr/Ca) and 0.4–0.7 mmol/mol (Mg/Ca). As is also observed in the portion of the shell grown in natural conditions, B/Ca is characterised by multi-day periods of reduced oscillation but elevated ratios, with a ~4 day period between 2.35 and 2.4 mm displaying ratios between 0.12 and 0.16 mmol/mol. In contrast to the NH growth period, Ba/Ca ratios show much clearer oscillations, while reduced and less clearly defined oscillations in Mg/Ca are more apparent than in the naturally grown part of the shell. El/Ca oscillations align well with daily growth bands present on the shell, with each of the 33 El/Ca peaks aligning with a corresponding dark growth band, yielding a daily growth rate of ~18.2 μm/day.

3.3. Imaging and long-term chronology

Both the slab and thin section of the shell show characteristic, distinct banding of alternating light-dark bands (Fig. 2). Furthermore, upon magnification daily growth increments are identifiable. The images obtained through microscope imaging and RLDI were viewed using the image editing software GIMP 2.10 to identify visible daily banding and manually obtain a counted chronology of the shell (Fig. 5). Given the aims of this study, we focused on the post-transition chronology of the shell within the aquarium setting.

Based on this daily growth banded chronology, the annual growth (mm) was measured and growth rate (μm/day) calculated, revealing a nonlinear growth through the lifetime of TS2 in the aquarium (Fig. 5). During the period 11/2001 to mid 2008 the shell is characterised by ~4 mm of annual growth (~10 μm/day), subsequently slowing substantially from ~2008 until TS2's death in late 2011, with a concomitant growth rate decrease to ~2.5 μm/day. This nonlinear growth is clearly expressed in the micrographs shown in Fig. 5A+B, wherein 0.5 mm of shell growth corresponds to ~26 and ~68 days of growth respectively.

The obtained chronology was used to place the El/Ca and stable isotope data onto an annual timescale for comparison with aquarium monitoring data. We note that while it has also been demonstrated that such a conversion can be achieved using daily chemical banding alone (Arndt et al., 2023), the loss of daily geochemical cyclicity in the shell following the transfer period precludes doing so in this case.

4. Discussion

In the following section, we discuss and interpret the most salient aspects of TS2's time-resolved sclerochemical record relative to the measured aquarium parameters, besides a general comparison to the findings in other studies.

4.1. Conversion of El/Ca and stable isotope data onto a sub-annual time scale

The obtained chronology allowed distance across the shell to be converted into time with a high degree of accuracy (Fig. 6). In turn, this enabled the comparison with ~10 years of aquarium monitoring data, which included aquarium water temperature, pH, water chemistry and salinity. Doing so demonstrates that the final ~3 years of life in the aquarium is represented by just the final ~3 mm of shell growth. Assessing the results in Fig. 3A and B in light of this, within the third period of variability, the interval between ~27–3 mm represents growth in the aquarium before seasonality (2002–2009) and ~3–0 mm occurred when a seasonal signal was introduced to the aquarium environment.

4.2. Comparison of time-resolved stable isotope and El/Ca data with aquarium parameters

4.2.1. Sclerochemistry prior- and post-introduction of artificial seasonality

Having been placed on a time axis, we observe little long-term variability in El/Ca from 2002 to mid-2005 such that the trace element data from this interval will not be discussed in detail here (Fig. 6). From mid-2006 onwards until the introduction of seasonality Mg/Ca begins to show greater variability, with several peaks occurring between 2007 and 2009, with an upward trend from 2008. Ba/Ca is characterised by a near doubling in 2007 to ~6 μmol/mol and Na/Ca appears to display cyclicity starting in ~2008. The $\delta^{18}O$ and $\delta^{13}C$ data of this period show unexpected shifts for a controlled aquarium environment prior to the introduction of artificial seasonality (Fig. 6). $\delta^{18}O$ displays a negative trend from ~2006 with a prominent negative spike in early 2007 of ~5 ‰, before the negative trend continues. $\delta^{13}C$ shows sudden variations between ~-4 to −8 ‰ from 2004 to 2007 followed by a negative trend.

The period of induced seasonality in the aquarium, between 2009 and 2012, corresponds to just the final ~3 mm of shell growth. During this interval, Mg/Ca appears to display some cyclicity from late 2009, while Sr/Ca and Na/Ca show clear cyclicity during this period. Little discernible structure exists in the $\delta^{18}O$ and $\delta^{13}C$ data which are both characterised by a plateau of ~-5 and ~-8 ‰ respectively. $\delta^{18}O$ shows some low amplitude oscillations during this time interval of ~0.5 ‰, between ~5.1 and 4.6 ‰, as to be expected given the induced seasonal temperature change in the aquarium.

Since it is a commonly used temperature proxy (Carpenter and Lohmann, 1995; Jouzel et al., 1994), the time-resolved $\delta^{18}O$ profile of TS2 was compared to the recorded aquarium water temperature. The aquarium water between 2001 and 2009 was characterised by a fairly constant temperature between ~25.8–26 °C, apart from some transient temperature peaks related to summer heatwaves of 2003, 2005 and 2006. From early 2009 onwards, the aquarium introduced artificial seasonality, varying the temperature between 25.0 and 26.5 °C (Fig. 7). Using the $\delta^{18}O$-temperature equation for aragonitic bivalves of Schöne et al. (2005), updated from Grossman and Ku (1986) and assuming consistent water chemistry, this seasonal variation in temperature is expected to correspond to a 0.3 ‰ range in $\delta^{18}O$ values. This theoretical

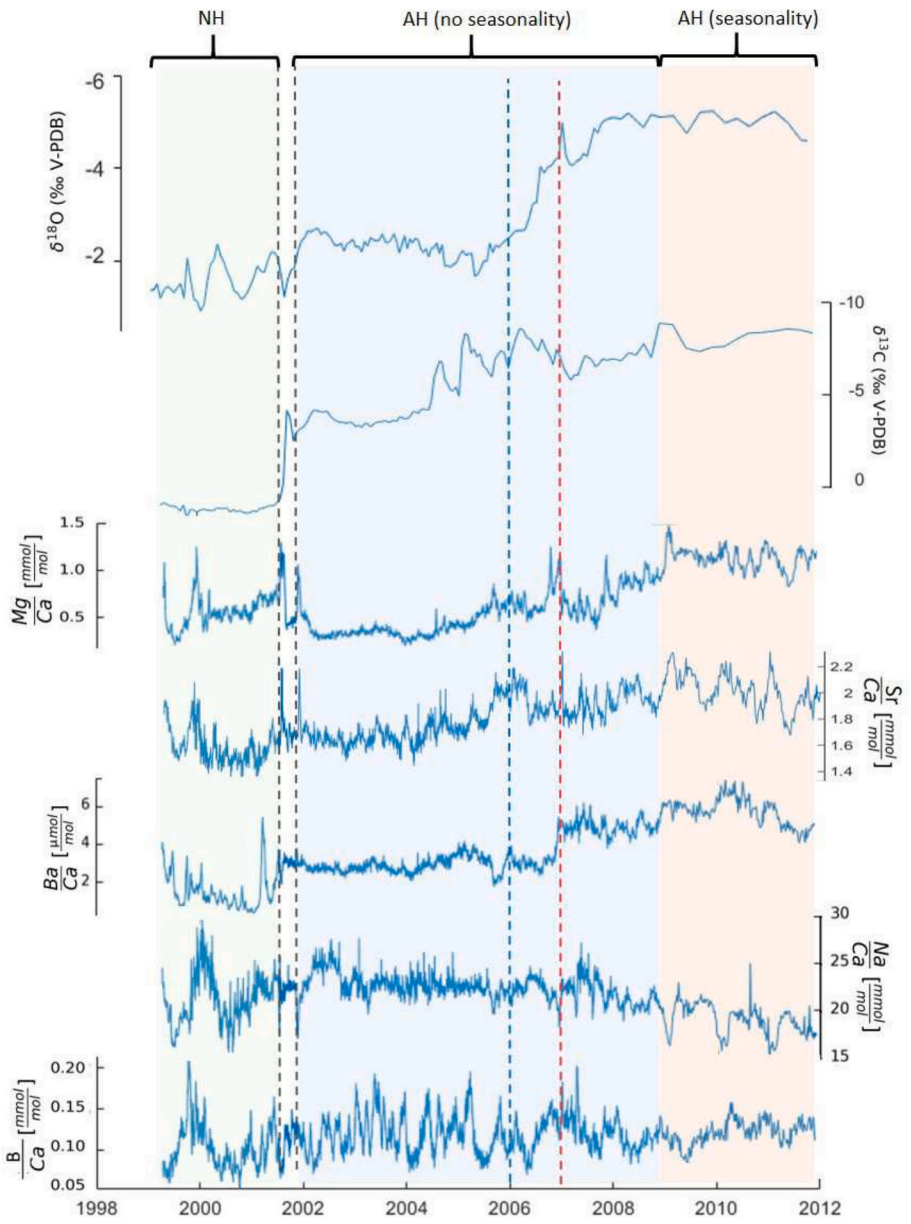

Fig. 6. Stable isotope and El/Ca results plotted against time. Background colouration indicates the time period of the life history of TS2 – Natural Habitat (green), Aquarium Habitat without seasonality (blue) and Aquarium Habitat with seasonality (yellow). The black dotted lines indicate the start and end of the Transition Period. The blue dotted line indicates the change in water change regime and the red dotted line indicates the nitrate spike. (For interpretation of the references to colour in this figure legend, the reader is referred to the web version of this article.)

assessment is close to the analytical precision and slightly lower than the observed ~0.5 ‰ variability in the shell (Fig. 7B). Given that shifts in the oxygen isotopic composition of the aquarium water are possible, we note that our results closely align with these theoretical values. The resolution of the shell data over this period is low due to the organism's low growth rate at this time coupled with the spatial resolution of the micromilling (220 m) which translates to only 3–4 $\delta^{18}O$ data points per year. However, we note that despite the slow growth rate, the induced temperature cyclicity is reflected in the growth banding of the shell, with darker bands correlating with colder periods (Fig. 7C).

While $\delta^{18}O$ and growth banding were found to be affected by temperature during the period of induced seasonality, overall the temperature was not the main control on shell $\delta^{18}O$ for TS2, especially regarding the shift to negative values in ~2006. We suggest that an alteration to water chemistry must have occurred in order to drive such trends. Using the $\delta^{18}O$-temperature equation of Schöne et al. (2005), and the recorded water temperature, we calculated the $\delta^{18}O$ of the aquarium water, according to:

$$\delta^{18}O_{seawater} = \delta^{18}O_{aragonite} - \left(\frac{20.60 - T(^{\circ}C)}{4.34}\right) + 0.2 \quad (1)$$

where T(°C) is the aquarium water temperature, and $\delta^{18}O_{aragonite}$ and $\delta^{18}O_{seawater}$ are the oxygen isotope composition of the shell sample and seawater relative to Vienna Pee Dee Belemnite (V-PDB) and Vienna Standard Mean Ocean Water (V-SMOW) respectively.

The corresponding results reveal a distinct shift in the $\delta^{18}O$ of the artificial seawater in the aquarium starting in 2006, from $\delta^{18}O_{seawater}$ of −1.0 to −3.8 ‰ (Fig. 8), with a concurrent shift also visible in the Ba/Ca data of TS2 (see below). According to the aquarium records, a change in the water exchange regime was introduced in 2006 (Supplementary Fig. 4), cycling out >100 % of the water annually through daily water changes, compared to only 40 % annually prior to this change (Janse

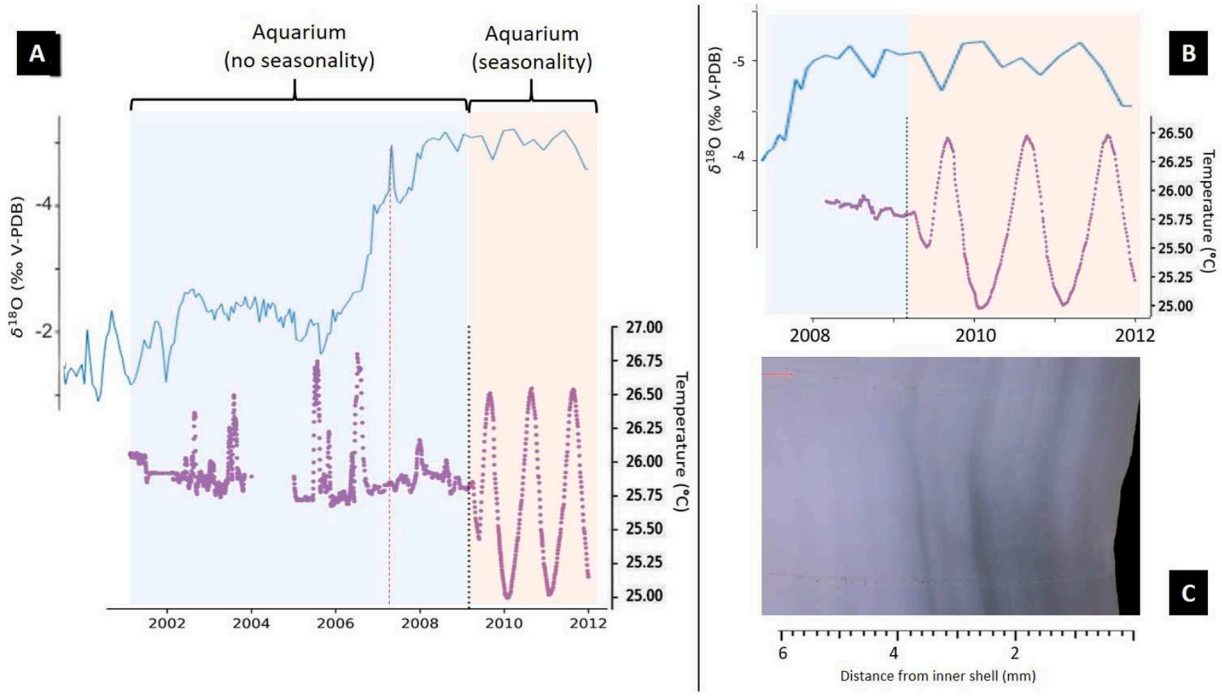

Fig. 7. (A) Shell $\delta^{18}O$ and aquarium temperature data (no aquarium data is available for 2004). Summer heatwaves in 2003, 2005 and 2006 are visible by spikes in temperature. The red line indicates the timing of the accidental nitrate spike (see text). (B) Enlargement of $\delta^{18}O$ and aquarium temperature data for the period of induced seasonality. (C) Portion of shell deposited during the time in which induced seasonality occurred. The dark banding aligns with the seasonal temperature data (panel B) demonstrating that these are deposited during cooler periods. (For interpretation of the references to colour in this figure legend, the reader is referred to the web version of this article.)

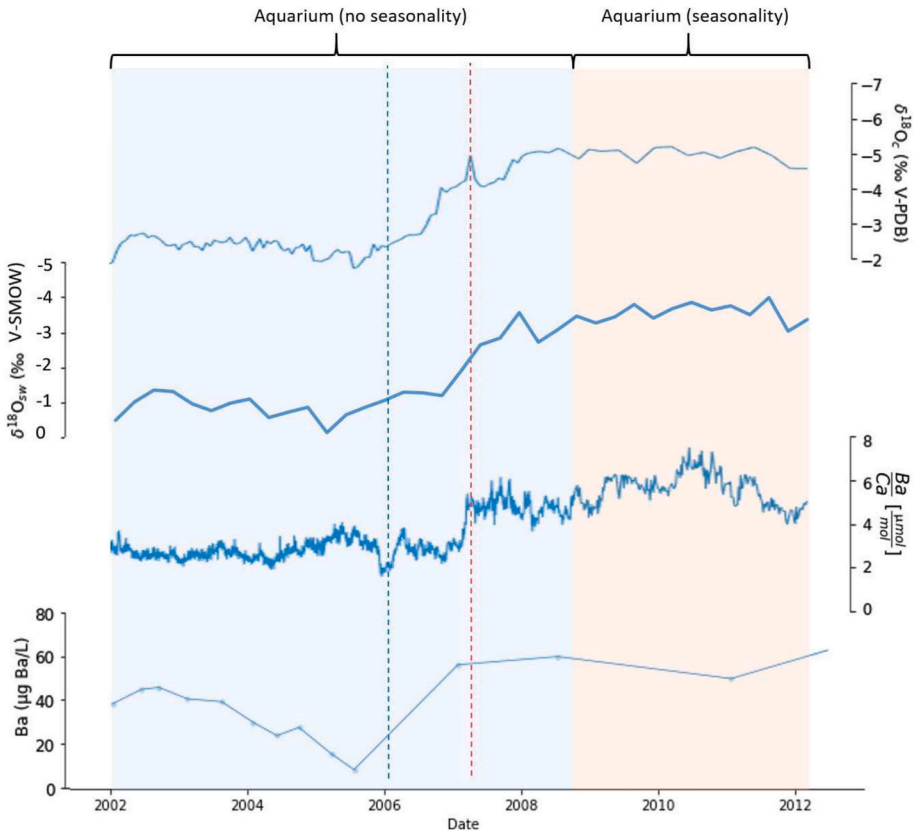

Fig. 8. Secular trends in $\delta^{18}O$ and Ba/Ca in TS2, as well as computed $\delta^{18}O$ of the aquarium seawater ($\delta^{18}O_{SW}$) and contextual aquarium water [Ba] data. The dashed blue and red lines indicate the change in water exchange regime and the accidental nitrate spike respectively. (For interpretation of the references to colour in this figure legend, the reader is referred to the web version of this article.)

et al., 2008). This change in the water replenishment regime coincides with the onset of the $\delta^{18}O$ shift, with the first complete change coming into effect in 2007. Despite using the same freshwater source to produce the artificial seawater throughout the life history of TS2, our $\delta^{18}O$ results suggest that some change in water composition has occurred. The change in water composition may potentially be a result of either a change in conditions at the water source, or some aspect of the water treatment process. Further evidence for a potential change in water composition can be seen in the shift in Ba/Ca ratios in TS2. Water chemistry records kept by the aquarium show that there was an increase in the addition of Ba^{2+} to the system between ~2006 and 2007 (see Supplementary Table S2), with a change in aquarium [Ba] from 10 to 60 μg Ba/L (Fig. 8), while seawater [Ca] remained nearly invariant (see Supplementary Table S3). The moderate positive correlation (R^2 value: 0.58) between the Ba/Ca and $\delta^{18}O$ of TS2 (Supplementary Fig. 5), suggest that a similar mechanism may have driven both shifts and the subsequent plateau.

Despite the existence of sharp SST peaks due to the summer heatwaves of 2003, 2005 and 2006 (Black et al., 2004; Rebetez et al., 2009; with a data gap in 2004), there is comparatively little $\delta^{18}O$ variation (~-2.5 to −2 ‰) between early 2002 and early 2006, apart from two fairly sharp excursions to less negative $\delta^{18}O$ values in mid-late 2005 (Fig. 7). These have the opposite direction to the more negative $\delta^{18}O$ values expected for higher SST, and thus likely reflect changes in $\delta^{18}O^{sw}$. The 2006 heatwave occurred during the water exchange regime change described above.

There is a steady decrease in $\delta^{13}C$ during TS2's life history after its introduction to the aquarium, from ~-3 to −8 ‰ which likely reflects some combination of changes in water composition (see above) and possible ontogenetic effects. Indeed, ontogenetic trends in $\delta^{13}C$ have been reported in several other bivalve species (Elliot et al., 2003; Jones et al., 1983; Keith et al., 1964; Krants et al., 1984; Romanek and Grossman, 1989; Yamanashi et al., 2016) and could be due to factors such as increased respiration or a shift in feeding habits of the organism. Lorrain et al. (2004) attributed this ontogenetic decrease to an increase in the incorporation of respiratory CO_2 as the size of the organism grows. That is, the larger the organism, the greater the degree of respiration and thus more metabolic, ^{12}C-enriched CO_2 available. Between 2005 and 2007 there are variations in $\delta^{13}C$ values between −5.0 and − 8.5 ‰. Such fluctuations are not seen elsewhere during the life history of the shell, either in natural conditions prior to 2001, or at any point later in the aquarium. While some studies have linked increased growth rate to C in aragonite secreting organisms with increased carbon demand for calcification leading to more negative $\delta^{13}C$ values (Klein et al., 1996; Lorrain et al., 2004; Ma et al., 2020; McConnaughey, 1989), it is unlikely that this is an explanation for the changes seen in TS2, given the magnitude of the change. While growth rate does change during the period of no induced seasonality, the variations seen in $\delta^{13}C$ do not align with this change, nor is the much sharper decrease in growth rate in 2008 reflected in shell $\delta^{13}C$. An alternative explanation may be an increase in filter feeding during this time, as such feeding has been shown to drive such variation in $\delta^{13}C$ values (Li et al., 2018; Rossi et al., 2004; Yang et al., 2019). It was indeed noted by aquarium staff that there was increased opening of the inhalation siphon of TS2 in the later years of its life. However, we do not possess the records of the aquarium carbon chemistry aside from the shell composition after the death of TS2, so cannot further interpret these results in detail.

We find no correlation between Mg/Ca and the induced seasonality in the AH, though the Mg/Ca ratio in bivalves, unlike coral aragonite, is known to be unaffected by changes in temperature (Marshall and McCulloch, 2001; Sinclair et al., 1998; Wei et al., 2000). Mg/Ca records a spike with the onset of induced artificial seasonality in 2009, followed by periodic variation from ~2010. The shift in aquarium settings could have been a stress event for the organism, resulting in the spike similar to those in the TP (see below) and stress events reported by other studies (Armstrong et al., 2022; Komagoe et al., 2018; Poulain et al., 2015; Warter et al., 2018; Yan et al., 2020; Zhao et al., 2023). While the aquarium began adding some Mg to the artificial seawater from 2005 (see Supp. Table S2), these additions are not reflected in TS2's overall Mg/Ca or the sub-annual Mg/Ca variability, with larger additions in later years causing no shifts in the Mg/Ca ratio, suggesting the addition of Mg to the aquarium water was not the prime cause and biological and/or kinetic factors likely affected the Mg/Ca uptake in TS2. Previous work has suggested that changes in Mg/Ca ratio reflects ontogenetic effects and are influenced by growth rate (Elliot et al., 2009; Romanek and Grossman, 1989; Warter et al., 2015, 2018). The overall increasing Mg/Ca ratio from late 2007 coincides with the decrease in growth rate of TS2 (Fig. 5), a phenomenon previously observed in other species of this genus (Arndt et al., 2023; Elliot et al., 2009). If we assume, as previous studies have found, that there is a link between increased Mg/Ca ratios and decreased growth rate (Arndt et al., 2023; Elliot et al., 2009; Romanek and Grossman, 1989; Warter et al., 2018; Warter et al., 2015), then this would explain our results. The oscillations from ~2010 onwards may be due to differences in growth between periods of warmer and colder induced seasonality.

Sr/Ca ratios between late 2001 and 2009 are characterised by low amplitude periodicity, with the biggest change occurring in the winter of 2005/06, which is noted as one of the coldest on record in recent history (Scaife and Knight, 2008). While some studies have suggested indirect links between Sr/Ca ratios with changes in SST (Warter et al., 2018; Yan et al., 2013, 2015; Zhou et al., 2022), we see no Sr/Ca change in line with the summer heatwaves reflected in the aquarium temperature, implying temperature is not a dominant control on Sr/Ca incorporation in TS2. While other studies have linked Sr/Ca incorporation to irradiance (Gillikin et al., 2005; Hori et al., 2015; Ip et al., 2017; Sano et al., 2012), light in the aquarium was kept constant each day using lamps, thereby discounting changes in irradiance as a factor responsible for the Sr/Ca variability observed in this specimen (Janse et al., 2008). As such, this implies that some other biophysiological factor is impacting or co-regulating the incorporation of Sr/Ca into the shell. While Sr^{2+} was added to the system from 2007 (See Supp. Table S1) to compensate for Sr incorporation during the growth of stony corals (Smith et al., 1979), the changes in Sr/Ca of TS2 do not reflect the timing nor amount of such additions. Sr/Ca shows a degree of variability during the induced temperature seasonality period and beyond, inverse to that of Na/Ca (Fig. 6). Some studies have suggested there may be a link between growth rate and Sr/Ca ratio (Arndt et al., 2025; Carré et al., 2006; Freitas et al., 2005; Gillikin et al., 2005; Klein et al., 1996; Purton et al., 1999; Stecher et al., 1996; Strasser et al., 2008; Takesue and van Geen, 2004). However, while there is a significant decrease in growth rate after the onset of induced seasonality (Fig. 5), the range of the Sr/Ca ratio is not different to that prior to it.

Between 2001 and 2007, B/Ca ratios display a variability between ~0.05–0.18 mmol/mol, after which this lessens to 0.10–0.15 mmol/mol (Fig. 9). While B/Ca has not been established as an environmental proxy in *Tridacna*, $\delta^{11}B$ is considered a promising pH proxy in foraminifera and coral studies (Babila et al., 2014; Coenen et al., 2024; Douville et al., 2010; Liu et al., 2015). As such, the B/Ca ratio has been assessed in comparison with the aquarium pH records, to examine whether it shows any such promise as a proxy for *Tridacna*. The pH of the aquarium is kept stable at 7.9 ± 0.15 (Janse et al., 2008), with variability slightly reduced to 7.9 ± 0.10 following the onset of the water exchange regime. It is unknown whether this slight reduction in pH variation and the B/Ca values reported here are causally related; further studies on the effect of pH on B/Ca incorporation are required to determine this.

Of the El/Ca ratios analysed, Na/Ca displays the clearest cyclicity during the period of induced seasonality (Fig. 6). A clear variability between ~15 and 20 mmol/mol is present between the induced cold and warm seasonality periods, respectively. Of the El/Ca ratios analysed, Na/Ca displays the clearest cyclicity during the period of induced seasonality (Fig. 10) with regular oscillations between ~16 and 21 mmol/mol present. Given that Na/Ca has been related to salinity in other

organisms such as foraminifera and some bivalves (Bertlich et al., 2018; Carvalho et al., 2019; Gray et al., 2023; Mezger et al., 2016), the salinity of the aquarium was assessed as a potential controlling parameter (Fig. 10). While aquarium salinity does show a roughly corresponding degree of cyclicity between ~33.8 and 34.2 on the practical scale, this began in ~2007, some two years before the onset of induced seasonality, and is not reflected in TS2's Na/Ca ratios prior to the introduction of seasonality. Moreover, during the TP, stress or irradiance seemed to be a driving factor decreasing shell Na/Ca. Hence, these data suggest that neither the salinity of the environment nor irradiance were major factors in the incorporation of sodium into the shell, but rather the reduced growth rate affected Na incorporation via some biological processes including organismal stress.

4.2.2. *Transition period – El/Ca peaks as markers of physiological stress*

The TP of the shell (~28–27 mm) occurred between summer and October of 2001 and is sclerochemically characterised by sharp and distinct variability in El/Ca and isotopic ratios that align with the clear dark banding of the shell (Fig. 6).

The most significant shift during this time is recorded in the $\delta^{13}C$ profile, as already noted by Batenburg et al. (2011) in another specimen, potentially due to differences in the carbon isotope composition between natural and artificial seawater. However, we also note that previous studies have found that $\delta^{13}C$ can be affected by the metabolic activity of symbiotic zooxanthellae in organisms such as corals or *Tridacna*. Due to their preferential removal of ^{12}C from ambient seawater, symbiotic activity results in an overall elevated $\delta^{13}C$ signature of the shell (Jones et al., 1986; Ma et al., 2020; McConnaughey and Gillikin, 2008; Romanek et al., 1987). Stress events have been found to have negative effects on zooxanthellae populations (Buck, 2000; Maboloc et al., 2015; Zhou et al., 2019). It is therefore possible that the stress event of being transported and introduced to a new environment had a negative effect on the zooxanthellae of TS2, requiring TS2 to rely, potentially solely, on filter feeding for its food, thus causing this significant negative $\delta^{13}C$ shift.

Mg/Ca and Sr/Ca are both characterised by sharp increases and Na/Ca by a decrease on either side of the TP as a response to the movement from natural conditions to the transfer container, and from the transfer container to the aquarium (Figs. 4 and 6). Previous studies have suggested that El/Ca peaks such as these are indicative of organismal stress (Armstrong et al., 2022; Komagoe et al., 2018; Poulain et al., 2015; Schleinkofer et al., 2021; Warter et al., 2018; Yan et al., 2020; Zhao et al., 2023). One study on blue mussels (*Mytilus edulis*) by Lorens and Bender (1980) hypothesised that in the case of Mg/Ca these high ratios may be the result of a temporary disruption to the Mg exclusion mechanism for the bivalve brought about by the stress of sudden adjustment to a new environment. As well as stress, irradiance may factor in these variations, as low light levels, which we can assume are likely during transportation of the specimen, have been linked with changes in El/Ca ratios. For example, a culturing study of *T. crocea* by Warter et al. (2018) showed that Mg/Ca values increased up to five-fold during low-light conditions as well as handling of the organism when transferring it into a new environment.

Previous works have suggested that there are strong biological controls on Sr/Ca ratios in many aragonite secreting organisms (Carré et al., 2006; Gillikin et al., 2005; Purton et al., 1999; Takesue and van Geen, 2004). While some studies have shown a temperature control on mollusc Sr/Ca, others indicate a correlation between low light levels with Sr/Ca peaks (Gillikin et al., 2005; Hori et al., 2015; Ip et al., 2017; Sano et al., 2012). Sano et al. (2012) hypothesise that the Sr/Ca ratio of the extrapallial fluid is higher at night, as the Ca^{2+}-ATPase pump is regulated by light activated enzymes. Warter et al. (2018) also found higher Sr/Ca ratios from shells cultured in complete darkness, further advancing this hypothesis.

In contrast to this, low light levels have been found to cause decreases in Na/Ca ratios, with studies showing that the transcription level and abundance of Na^+/H^+ exchanger proteins are affected by factors such as irradiance, though insolation may be potentially indirectly affecting Na/Ca through its effect on growth rate (Boo et al., 2017, 2019; Hiong et al., 2017). The sudden increase in Mg/Ca and Sr/Ca aligned with the Na/Ca decreases during either side of the TP would align with the assumption that the organism was kept in low-light conditions during the immediate transfer from the NH and into the AH.

Ba/Ca shows no peaks during the TP when measured at lower temporal resolution (Fig. 6), however at daily resolution there appear to be spikes around the onset of the TP. An increase in Ba/Ca visible immediately prior to transition may relate to a change in seawater composition prior to collection driven by freshwater input (Cao et al., 2023; Elliot et al., 2009; Gillikin et al., 2006; Poulain et al., 2015). The rainy season for the majority of Vietnam reaches its highest levels of

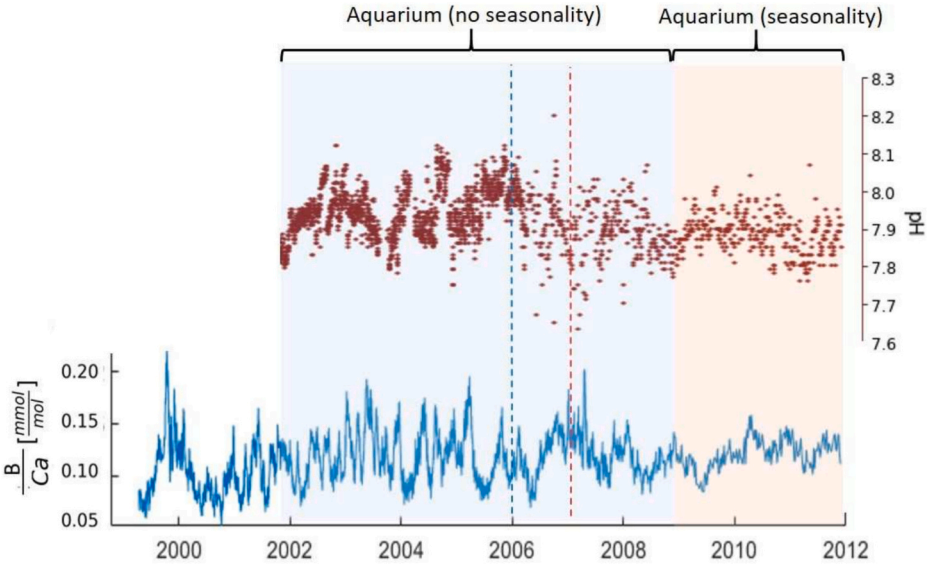

Fig. 9. Time-resolved profiles of aquarium pH (using a weekly moving average of the data) and B/Ca data of TS2. The dashed blue line indicates the start of the water exchange regime change and the red line indicated the nitrate spike. Blue colouration signifies the period of time of life history of TS2 in the Aquarium Habitat without seasonality, while pink signifies time in the Aquarium Habitat with seasonality. (For interpretation of the references to colour in this figure legend, the reader is referred to the web version of this article.)

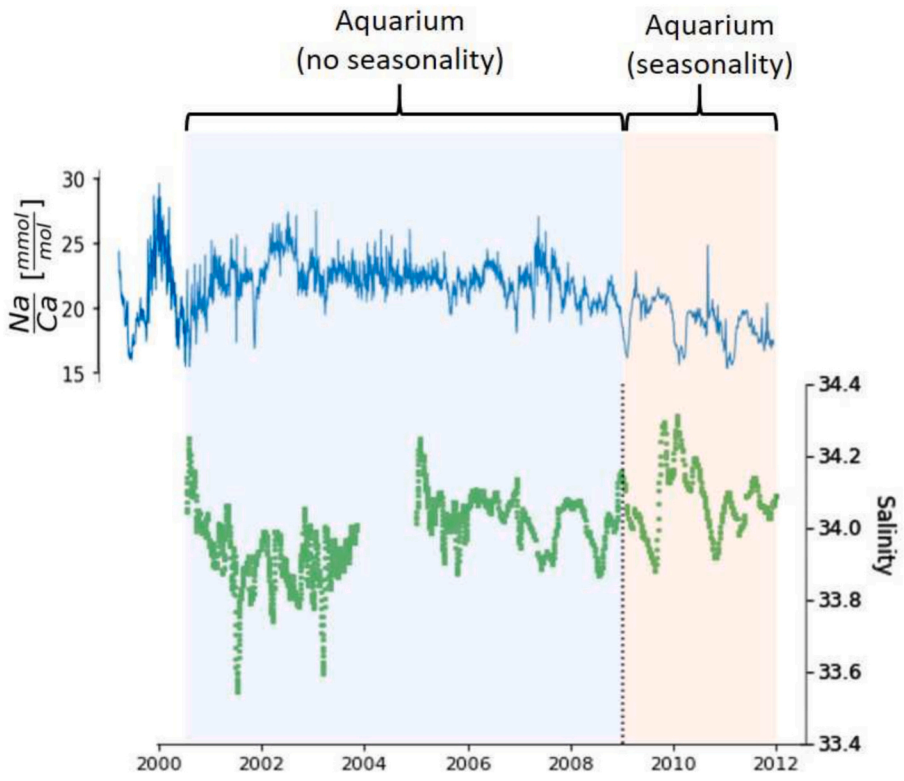

Fig. 10. Na/Ca ratio of TS2 (blue) compared to aquarium salinity values (green). Blue colouration signifies period of time of life history of TS2 in the AH without seasonality, yellow signifying time in the AH with seasonality. (B) Close up of results at the onset of seasonality. Oscillations in Na/Ca are clear from the onset of seasonality. However, minor variability in aquarium salinity predate this, starting ~2007.

precipitation in July – August (Iponre, 2009; Ngo-Duc, 2014), the time during which it is thought TS2 was collected, and so freshwater input from increased precipitation may account for this first peak. However, the second peak, correlating with the other El/Ca peaks, is of the same intensity as the first Ba/Ca peak, suggesting that organismal stress may have accounted for these peaks and play a factor in Ba/Ca incorporation in *Tridacna*. Following this spike the Ba/Ca ratio is 2–3-fold higher than the Vietnamese NH, which broadly is also the case during the initial years in the aquarium (Fig. 6). This is in-line with a slightly higher than natural seawater [Ba] in the aquarium, as discussed earlier (Fig. 8).

The B/Ca ratio appears to be the least affected by the TP, showing similar variations between 0.05 and 0.17 mmol/mol between ~2001–2006, a period covering the shell's life history in the NH, the TP and the AH. Stress events such as the TP, which affected El/Ca ratios such as Mg, Sr and Na, do not coincide with B/Ca ratio variations for TS2. While previous studies on B/Ca have shown no clear connection with factors such as irradiance (Warter et al., 2018), mirrored by our results, some studies have shown links between B/Ca ratios and the seawater carbonate system in other calcifying organisms, which we cannot assess here as we lack the necessary seawater data (Hemming and Hanson, 1992; Sanyal et al., 2000; Yu et al., 2010).

The change in growth rate between the three periods (NH, TP and AH), from ~22.0 μm/day in NH, to ~7.0 μm/day during the TP, to ~18.2 μm/day in the AH, indicates that there are strong environmental factors that affect the rate of growth (Fig. 4). Conditions during the transfer are unknown, but previous studies have shown that periods of significantly lower growth rates are indicative of periods of organismal stress (Armstrong et al., 2022; Elfwing et al., 2001, 2003; Poulain et al., 2015; Warter et al., 2018), such that we hypothesise that this significant change in growth rate during the TP is indicative of a period of organismal stress during transportation.

In both NH and AH there is clear periodic variability in El/Ca ratios, indicative of daily cycles in environmental conditions or physiology, which align with the banding present in the shell. In contrast, during the TP there is a lack of cyclicity of any form present in all El/Ca ratios (with the possible exception of Sr/Ca) and no distinct banding visible. Cyclicity of El/Ca ratios in *Tridacna* has been shown to be driven by various biophysiological mechanisms which are modulated by conditions such as temperature, pH, the diurnal light cycle and diurnal changes in the biological activity of the organism; these conditions have been shown to coincide with daily banding secreted by the shell (Arndt et al., 2023; Duprey et al., 2015; Gannon et al., 2017; Warter et al., 2018; Zhao et al., 2023). The NH and AH show clear correlation between the upward periods of cyclicity in El/Ca ratios and the light section of each light/dark coupling of a daily growth band. This strict and clear cyclicity, especially in Mg/Ca and Sr/Ca, suggests diurnal conditions affecting El/Ca ratios, which would be consistent with factors such as temperature and irradiance driving the incorporation of different elements (Hiong et al., 2017; Ma et al., 2020; Mills et al., 2024; Sano et al., 2012; Warter et al., 2018; Warter et al., 2018; de Winter et al., 2022).

Assuming that increased El/Ca ratios reflect organismal stress and that the high Mg/Ca and Sr/Ca peaks at the onset and end of the TP are stress induced, then one might expect similarly high El/Ca levels during the middle section of the TP to indicate this stress. Whereas in fact, the Mg/Ca and Sr/Ca ratios during the middle section of the TP show values not overly dissimilar to those in the NH or AH, at less than 1 mmol/mol and 2 mmol/mol respectively. This has implications for the link between organismal stress, El/Ca ratios and growth rate. Although growth rate is significantly slowed, presumably indicating that organismal stress is high, the El/Ca ratios have returned to roughly natural levels. This implies that organismal stress may be linked to growth rate and El/Ca ratios on different time scales, with stress manifesting itself in shell sclerochemistry in discrete peaks rather than long-term changes. This is a concept that would warrant further testing through future specific culturing studies.

4.3. Nitrate spike

The accidental addition of excess sodium nitrate instead of sodium carbonate in January 2007 led to a nearly 50-fold increase in NO_3^- from ~0.05 to ~2.4 mg/l (Janse et al., 2008) (Supplementary Fig. 6). While it was reported by Janse et al. (2008) that limited adverse effects were seen on the coral population, it took ~six months for the nitrate levels to decrease again. Nitrate is considered the least toxic of inorganic nitrogen species in aquarium settings, however, there can still be adverse effects in fish and amphibian species from elevated concentrations (Brown, 1987; Hecnar, 1995; Muir et al., 1991; Tal et al., 2003). While the reaction of *Tridacna* to such elevated levels has, to our knowledge, not been previously examined, studies have shown that corals and their zooxanthellae are more resilient to higher nitrate levels, tolerating limited nitrification for short periods of time of up to a month, as long as it is not coupled with extreme warming events (Koop et al., 2001; Schlöder and D'Croz, 2004). The sclerochemistry of TS2 shows that during this spike there were also spikes in Mg/Ca and Sr/Ca, as well as a negative spike in Na/Ca (Fig. 6). Based on our discussion of El/Ca ratio peaks as biomarkers of organismal stress during the TP (see above), we can assume that the peaks seen here are the result of similar stresses induced by the nitrate spike, especially with regards to Mg/Ca ratios. While irradiance was cited as a potential factor influencing Sr/Ca and Na/Ca ratios, this stress event at constant temperature and light conditions suggests that there are further biophysiological factors that can influence these ratios. Although the Mg/Ca spike was equal in amplitude to those experienced in the TP, the coeval dark banding does not display the same intensity, suggesting that although studies have linked high Mg/Ca ratios with shell banding (Arndt et al., 2023; Warter et al., 2015), factors such as the duration of the stress period (impacting shell growth rate and therefore density) are the key controls on banding visibility. Furthermore there is a Mg/Ca spike of equal intensity just prior to the nitrate spike, as well as overall similar Mg/Ca and Sr/Ca ratios later in the life history. This suggests the nitrate spike may not be a primary cause of sclerochemical change, but rather that another environmental condition drove such shifts, potentially through organismal stress. Ba/Ca is characterised by an increase at this time, but we consider this to be coincidental as the nitrate spike coincides with the end of the first cycle of the water change regime, which we hypothesise is more likely to be the causal driver of this Ba/Ca peak.

Overall, $\delta^{18}O$ values trend towards more negative values at this time in the life history of TS2, driven by a change in the isotopic composition of seawater. However, the nitrate spike coincides with a sharp excursion towards more negative $\delta^{18}O$ values on top of this during constant aquarium SST and on a timescale that is unlikely to be driven by $\delta^{18}O^{sw}$ (Fig. 7A). Studies on the incorporation of nitrate $\delta^{18}O$ into marine organisms would be needed to assess whether the nitrate additions can cause a change in *Tridacna* $\delta^{18}O$. While studies have linked more negative $\delta^{18}O$ signals in soil to nitrate fertilisers (Ansari et al., 2023; Fang et al., 2012; Ji et al., 2022; Loo et al., 2017), the $\delta^{18}O$ spike seen here may well exceed what would be accounted for by the accidental addition of sodium nitrate to the aquarium.

5. Conclusions

This study reports, to the best of our knowledge, the results of a unique decade-long experiment that compares time-resolved *Tridacna* sclerochemistry of a sample (TS2) that lived for a few years in its natural environment before being transferred to a zoo aquarium comprised of tightly monitored parameters in a quasi-controlled environment. Thanks to intended and unintended changes affecting the aquarium conditions, such as long-term variations to the water exchange regime, an accidental NO_3^- spike or the induced temperature seasonality, we can better assess some environmental parameters affecting the shell composition. However, the influences on the the oxygen and carbon isotopic and elemental composition in *Tridacna* are complex and driven by multiple factors such that it is difficult to be definitive on the impact of environmental parameters on the sclerochemistry.

In this tightly controlled setting, we are able to identify that large changes in TS2's $\delta^{18}O$ record are caused by changes to the water exchange regime of the aquarium and related $\delta^{18}O^{sw}$, but cannot identify with any certainty what causes the observed transient $\delta^{18}O$ spikes such as during the brief accidental (NO_3^-) addition. We could not resolve the aquarium's induced 1.5 °C temperature seasonality in the microsampled $\delta^{18}O$ profile due to the strongly reduced growth rate during TS2's final three years that resulted in insufficient sampling resolution. The variable $\delta^{13}C$ record was found to be difficult to interpret without detailed information about the aquarium's carbon(ate) water chemistry.

Organismal stress affecting El/Ca especially during the TP is clearly demonstrated by the high-spatial resolution analysis. The stress that organism handling and new environments have on *Tridacna* is clearly reflected in El/Ca ratios visible as positive spikes in Mg/Ca and Sr/Ca and negative spikes in Na/Ca, as shown or suggested by previous studies (Poulain et al., 2015; Warter et al., 2018). However, while the reduction in growth rate due to adverse conditions is apparent, the El/Ca ratios after the initial stress spikes with similar values to natural and/or aquarium conditions indicate that *Tridacna* are potentially capable of adaptation to temporarily unfavourable conditions in terms of their calcification site chemistry, although shell extension rate never recovered to pre-collection values. The increased/decreased El/Ca values as well as the reduced growth rate are also present after the introduction of seasonality in the aquarium, demonstrating that an artificial lack of environmental variability was not the only cause of stress that the organism faced following collection.

Moreover, this study has shown (once again) that obtaining a good chronological control is of vital importance for sclerochemical studies, as the conversion of TS2's distance-resolved data to time-resolved data is necessary to obtain an understanding of the effect that external environmental factors have on the organism. Dark field illumination was found to be of particular effective in obtaining images with a good degree of contrast for chronological counting, especially in low growth domains.

Overall, TS2's decade-long record shows clearly that for a sample that experienced only limited to no environmental variability for several years, the sclerochemical profiles can display remarkable degrees of heterogeneity. Further culturing studies, both long- and short-term, under controlled conditions are necessary to better disentangle the relationships between various sclerochemical changes and environmental parameters and/or biophysiological processes. Only then can we better identify control parameters in natural samples that display significant degrees of compositional variability.

CRediT authorship contribution statement

Max Fursman: Writing – review & editing, Writing – original draft, Visualization, Investigation, Formal analysis, Data curation. **Viola Warter:** Writing – review & editing, Validation, Project administration, Investigation, Formal analysis, Data curation. **Max Janse:** Writing – review & editing, Validation, Resources. **Willem Renema:** Writing – review & editing, Validation, Project administration, Funding acquisition. **Christoph Spötl:** Writing – review & editing, Validation, Methodology. **Iris Arndt:** Writing – review & editing, Validation. **David Evans:** Writing – review & editing, Validation, Supervision, Methodology. **Wolfgang Müller:** Writing – review & editing, Validation, Supervision, Project administration, Methodology, Funding acquisition, Conceptualization.

Declaration of competing interest

The authors declare no competing interests or personal relationships that could have appeared to influence the work reported in this paper.

Acknowledgements

We are grateful for funding of the European Union's Horizon 2020 Marie Skłodowska-Curie grant agreement (4D-REEF, No 813360). We thank Wolfgang Schiller for assistance with the reflected light darkfield photography of the sample. Some data presented herein were generated at Wolfgang Müller's previous institution, Royal Holloway University of London, where LA-ICPMS instrumentation was funded by SRIF3 (HEFCE, 2008) and NERC (NERC CC073; 2014) equipment grants, for which we are grateful. At Frankfurt, FIERCE is financially supported by the Wilhelm and Else Heraeus Foundation and by the Deutsche Forschungsgemeinschaft (DFG: INST 161/921-1 FUGG, INST 161/923-1 FUGG and INST 161/1073-1 FUGG), which is gratefully acknowledged. This is FIERCE contribution No. 201. We thank the Royal Burgers' Zoo Aquarium team for their extended care of the coral reef tank, and the lab manager Manuela Wimmer at the University of Innsbruck for help with stable isotope analysis.

Appendix A. Supplementary data

Supplementary data to this article can be found online at https://doi.org/10.1016/j.palaeo.2025.113022.

Data availability

All datasets are available in the main text and supplementary materials.

References

Aharon, P., 1983. Carbon and oxygen isotope probes of reef environment histories. In: Perspectives on Coral Reefs. Austral. Inst. Mar. Sci.

Aharon, P., 1991. Recorders of reef environment histories: stable isotopes in corals, giant clams, and calcareous algae. Coral Reefs 10, 71–90. https://doi.org/10.1007/BF00571826.

Aharon, P., Chappell, J., 1986. Oxygen isotopes, sea level changes and the temperature history of a coral reef environment in new guinea over the last 105 years. Palaeogeogr. Palaeoclimatol. Palaeoecol. 56, 337–379. https://doi.org/10.1016/0031-0182(86)90101-X.

Alibert, C., McCulloch, M.T., 1997. Strontium/calcium ratios in modern porites corals from the Great Barrier Reef as a proxy for sea surface temperature: calibration of the thermometer and monitoring of ENSO. Paleoceanography 12, 345–363. https://doi.org/10.1029/97PA00318.

Ansari, M.A., Saravana Kumar, U., Noble, J., Akhtar, N., Akhtar, M.A., Deodhar, A., 2023. Isotope hydrology tools in the assessment of arsenic contamination in groundwater: an overview. Chemosphere 340, 139898. https://doi.org/10.1016/j.chemosphere.2023.139898.

Armstrong, E.J., Watson, S.A., Stillman, J.H., Calosi, P., 2022. Elevated temperature and carbon dioxide levels alter growth rates and shell composition in the fluted giant clam, *Tridacna squamosa*. Sci. Rep. 12, 1–17. https://doi.org/10.1038/s41598-022-14503-4.

Arndt, I., Coenen, D., Evans, D., Renema, W., Müller, W., 2023. Quantifying sub-seasonal growth rate changes in fossil giant clams using wavelet transformation of daily Mg/Ca cycles. Geochem. Geophys. Geosyst. 24, e2023GC010992. https://doi.org/10.1029/2023GC010992.

Arndt, I., Bernecker, M., Erhardt, T., Evans, D., Fiebig, J., Fursman, M., Kniest, J., Renema, W., Schlidt, V., Staudigel, P., Voigt, S., 2025. 20,000 days in the life of a giant clam reveal late Miocene tropical climate variability. Palaeogeogr. Palaeoclimatol. Palaeoecol. 661, 112711.

Ayling, B.F., Chappell, J., Gagan, M.K., McCulloch, M.T., 2015. ENSO variability during MIS 11 (424-374 ka) from Tridacna gigas at Huon Peninsula, Papua New Guinea. Earth Planet. Sci. Lett. 431, 236–246. https://doi.org/10.1016/j.epsl.2015.09.037.

Babila, T.L., Rosenthal, Y., Conte, M.H., 2014. Evaluation of the biogeochemical controls on B/Ca of Globigerinoides ruber white from the Oceanic Flux Program, Bermuda. Earth Planet. Sci. Lett. 404, 67–76. https://doi.org/10.1016/j.epsl.2014.05.053.

Batenburg, S.J., Reichart, G.J., Jilbert, T., Janse, M., Wesselingh, F.P., Renema, W., 2011. Interannual climate variability in the Miocene: high resolution trace element and stable isotope ratios in giant clams. Palaeogeogr. Palaeoclimatol. Palaeoecol. 306, 75–81. https://doi.org/10.1016/j.palaeo.2011.03.031.

Bertlich, J., Nürnberg, D., Hathorne, E.C., De Nooijer, L.J., Mezger, E.M., Kienast, M., Nordhausen, S., Reichart, G.J., Schönfeld, J., Bijma, J., 2018. Salinity control on na incorporation into calcite tests of the planktonic foraminifera trilobatus sacculifer–evidence from culture experiments and surface sediments. Biogeosciences 15, 5991–6018.

Black, E., Blackburn, M., Harrison, G., Hoskins, B., Methven, J., 2004. Factors contributing to the summer 2003 european heatwave. Weather 59, 217–223. https://doi.org/10.1256/wea.74.04.

Bonham, K., 1965. Growth rate of giant clam *tridacna gigas* at bikini atoll as revealed by radioautography. Science 149, 300–302. https://doi.org/10.1126/science.149.3681.300.

Boo, M.V., Hiong, K.C., Choo, C.Y., Cao-Pham, A.H., Wong, W.P., Chew, S.F., Ip, Y.K., 2017. The inner mantle of the giant clam, *Tridacna squamosa*, expresses a basolateral Na^+/K^+-ATPase α-subunit, which displays light-dependent gene and protein expression along the shell-facing epithelium. PLoS One 12, 1–21. https://doi.org/10.1371/journal.pone.0186865.

Boo, M.V., Hiong, K.C., Wong, W.P., Chew, S.F., Ip, Y.K., 2019. Shell formation in the giant clam, *Tridacna squamosa*, may involve an apical Na^+/Ca^{2+} exchanger 3 homolog in the shell-facing epithelium of the whitish inner mantle, which displays light-enhanced gene and protein expression. Coral Reefs 38, 1173–1186. https://doi.org/10.1007/s00338-019-01848-y.

Brown, B.E., 1987. Worldwide death of corals-natural cyclical events or man-made pollution? Mar. Pollut. Bull. 18, 9–13. https://doi.org/10.1016/0025-326X(87)90649-7.

Buck, B.H., 2000. Experimentally Induced Bleaching and Recovery of Tridacna Gigas. Doctoral Dissertation. University of Bremen.

Cao, J., Yang, S., Tang, D., Feng, J., Liang, J., 2023. Mg/Ca, Ba/Ca, and S/Ca ratios as environmental and growth proxies for bivalve shells from the Haima cold seep, South China Sea. J. Oceanol. Limnol. 41, 660–672. https://doi.org/10.1007/s00343-022-2010-8.

Carpenter, S.J., Lohmann, K.C., 1995. $\delta_{18}O$ and $\delta_{13}C$ values of modern brachiopod shells. Geochim. Cosmochim. Acta 59, 3749–3764. https://doi.org/10.1016/0016-7037(95)00291-7.

Carré, M., Bentaleb, I., Bruguier, O., Ordinola, E., Barrett, N.T., Fontugne, M., 2006. Calcification rate influence on trace element concentrations in aragonitic bivalve shells: evidences and mechanisms. Geochim. Cosmochim. Acta 70, 4906–4920. https://doi.org/10.1016/j.gca.2006.07.019.

Carvalho, A., Gomes, I., Swearer, S.E., Queiroga, H., Peteiro, L.G., 2019. Temperature and salinity influence on element incorporation into *mytilus galloprovincialis* larvae shells: discerning physiological from environmental control. Mar. Ecol. Prog. Ser. 626, 83–96.

Chauvaud, L., Lorrain, A., Dunbar, R.B., Paulet, Y.M., Thouzeau, G., Jean, F., Guarini, J. M., Mucciarone, D., 2005. Shell of the great scallop *pecten maximus* as a high-frequency archive of paleoenvironmental changes. Geochem. Geophys. Geosyst. 6. https://doi.org/10.1029/2004GC000890.

Coenen, D., Evans, D., Hauzer, H., Nambiar, R., Jurikova, H., Dumont, M., Kanna, P., Rae, J., Erez, J., Cotton, L., Renema, W., 2024. Boron isotope pH calibration of a shallow dwelling benthic nummulitid foraminifera. Geochimica et Cosmochimica Acta 378, 217–233. https://doi.org/10.1016/j.gca.2024.06.020.

Comfort, A., 1957. The duration of life in molluscs. J. Molluscan Stud. 32, 219–241. https://doi.org/10.1093/oxfordjournals.mollus.a064785.

de Winter, N.J., Killam, D., Fröhlich, L., de Nooijer, L., Boer, W., Schöne, B.R., Thébault, J., Reichart, G.J., 2022. Ultradian rhythms in shell composition of photosymbiotic and non-photosymbiotic mollusks. EGUsphere 2. https://doi.org/10.5194/bg-20-3027-2023.

Douville, É., Paterne, M., Cabioch, G., Louvat, P., Gaillardet, J., Juillet-Leclerc, A., Ayliffe, L., 2010. Abrupt sea surface pH change at the end of the Younger Dryas in the central sub-equatorial Pacific inferred from boron isotope abundance in corals (Porites). Biogeosciences 7 (8), 2445–2459. https://doi.org/10.5194/bg-7-2445-2010.

Duprey, N., Lazareth, C.E., Dupouy, C., Butscher, J., Farman, R., Maes, C., Cabioch, G., 2015. Calibration of seawater temperature and $\delta_{18}O$seawater signals in Tridacna maxima's $\delta_{18}O$shell record based on in situ data. Coral Reefs 34, 437–450. https://doi.org/10.1007/s00338-014-1245-z.

Eckman, W., Vicentuan, K., Todd, P.A., 2019. Effects of low light and high temperature on pediveligers of the fluted giant clam *Tridacna squamosa*. Mar. Freshw. Behav. Physiol. 52, 255–264. https://doi.org/10.1080/10236244.2019.1700117.

Elfwing, T., Plantman, P., Tedengren, M., Wijnbladh, E., 2001. Responses to temperature, heavy metal and sediment stress by the giant clam *Tridacna squamosa*. Mar. Freshw. Behav. Physiol. 34, 239–248. https://doi.org/10.1080/10236240109379077.

Elfwing, T., Blidberg, E., Sison, M., Tedengren, M., 2003. A comparison between sites of growth, physiological performance and stress responses in transplanted *Tridacna gigas*. Aquaculture 219, 815–828. https://doi.org/10.1016/S0044-8486(02)00660-9.

Elliot, M., DeMenocal, P.B., Linsley, B.K., Howe, S.S., 2003. Environmental controls on the stable isotopic composition of *Mercenaria mercenaria*: potential application to paleoenvironmental studies. Geochem. Geophys. Geosyst. 4. https://doi.org/10.1029/2002GC000425.

Elliot, M., Welsh, K., Chilcott, C., McCulloch, M., Chappell, J., Ayling, B., 2009. Profiles of trace elements and stable isotopes derived from giant long-lived *Tridacna gigas* bivalves: potential applications in paleoclimate studies. Palaeogeogr. Palaeoclimatol. Palaeoecol. 280, 132–142. https://doi.org/10.1016/j.palaeo.2009.06.007.

Estacion, J., Braley, R.D., 1988. Growth and survival of *Tridacna gigas* juveniles in an intertidal pond. ACIAR Monograph 9, 191–192.

Evans, D., Müller, W., 2018. Automated extraction of a five-year LA-ICP-MS trace element data set of ten common glass and carbonate reference materials: Long-term data quality, optimisation and laser cell homogeneity. Geostandards and Geoanalytical Research 42 (2), 159–188.

Fang, Y., Koba, K., Makabe, A., Zhu, F., Fan, S., Liu, X., Yoh, M., 2012. Low $\delta_{18}O$ values of nitrate produced from nitrification in temperate forest soils. Environ. Sci. Technol. 46, 8723–8730. https://doi.org/10.1021/es300510r.

Faylona, M.G.P.G., Lazareth, C.E., Sémah, A.M., Caquineau, S., Boucher, H., Ronquillo, W.P., 2011. Preliminary study on the preservation of giant clam

(*Tridacnidae*) shells from the Balobok Rockshelter archaeological site, South Philippines. Geoarchaeology 26, 888–901. https://doi.org/10.1002/gea.20377.
Freitas, P., Clarke, L.J., Kennedy, H., Richardson, C., Abrantes, F., 2005. Mg/ca, sr/ca, and stable-isotope ($\delta_{18}O$ and $\delta_{13}C$) ratio profiles from the fan mussel *pinna nobilis*: seasonal records and temperature relationships. Geochem. Geophys. Geosyst. 6. https://doi.org/10.1029/2004GC000872.
Gannon, M.E., Pérez-Huerta, A., Aharon, P., Street, S.C., 2017. A biomineralization study of the Indo-Pacific giant clam *Tridacna gigas*. Coral Reefs 36, 503–517. https://doi.org/10.1007/s00338-016-1538-5.
Gillikin, D.P., Lorrain, A., Navez, J., Taylor, J.W., André, L., Keppens, E., Baeyens, W., Dehairs, F., 2005. Strong biological controls on Sr/Ca ratios in aragonitic marine bivalve shells. Geochem. Geophys. Geosyst. 6. https://doi.org/10.1029/2004GC000874.
Gillikin, D.P., Dehairs, F., Lorrain, A., Steenmans, D., Baeyens, W., André, L., 2006. Barium uptake into the shells of the common mussel (*mytilus edulis*) and the potential for estuarine paleo-chemistry reconstruction. Geochim. Cosmochim. Acta 70, 395–407. https://doi.org/10.1016/j.gca.2005.09.015.
Gomez, E., Belda, C., 1988. Growth of giant clams in bolinao, Philippines. Giant clams in Asia and the Pacific. AClAR Monograph 9, 178–182.
Goodwin, D.H., Flessa, K.W., Schone, B.R., Dettman, D.L., 2001. Cross-calibration of daily growth increments, stable isotope variation, and temperaturre in the Gulf of California Bivalve Mollusck *Chione cortezi*: implications for paleoenvironmental analysis. Palaios 16, 387–398. https://doi.org/10.1669/0883-1351(2001)016<0387:CCODGI>2.0.CO;2.
Goodwin, D.H., Schöne, B.R., Dettman, D.L., 2003. Resolution and fidelity of oxygen isotopes as paleotemperature proxies in bivalve mollusk shells: models and observations. Palaios 18, 110–125. https://doi.org/10.1669/0883-1351(2003)18<110:RAFOOI>2.0.CO;2.
Gornitz, V., 2009. Encyclopedia of Paleoclimatology and Ancient Environments. Springer Science & Business Media.
Gray, W.R., Evans, D., Henehan, M., Weldeab, S., Lea, D.W., Müller, W., Rosenthal, Y., 2023. Sodium incorporation in foraminiferal calcite: an evaluation of the na/ca salinity proxy and evidence for multiple na-bearing phases. Geochim. Cosmochim. Acta 348, 152–164.
Gröcke, D.R., Gillikin, D.P., 2008. Advances in mollusc sclerochronology and sclerochemistry: tools for understanding climate and environment. Geo-Mar. Lett. 28, 265–268. https://doi.org/10.1007/s00367-008-0108-4.
Grossman, E.L., Ku, T.L., 1986. Oxygen and carbon isotope fractionation in biogenic aragonite: temperature effects. Chemical Geology: Isotope Geoscience Section 59, 59–74. https://doi.org/10.1016/0168-9622(86)90057-6.
Harzhauser, M., Mandic, O., Piller, W.E., Reuter, M., Kroh, A., 2008. Tracing back the origin of the indo-pacific mollusc fauna: Basal *tridacninae* from the oligocene and miocene of the Sultanate of oman. Palaeontology 51, 199–213. https://doi.org/10.1111/j.1475-4983.2007.00742.x.
Hecnar, S.J., 1995. Acute and chronic toxicity of ammonium nitrate fertilizer to amphibians from southern Ontario. Environ. Toxicol. Chem. 14, 2131–2137. https://doi.org/10.1002/etc.5620141217.
Hemming, N.G., Hanson, G.N., 1992. Boron isotopic composition and concentration in modern marine carbonates. Geochim. Cosmochim. Acta 56, 537–543. https://doi.org/10.1016/0016-7037(92)90151-8.
Henderson, G.M., 2002. New oceanic proxies for paleoclimate. Earth Planet. Sci. Lett. 203, 1–13. https://doi.org/10.1016/S0012-821X(02)00809-9.
Heslinga, G.A., Perron, F.E., Orak, O., 1984. Mass culture of giant clams (F. *Tridacnidae*) in Palau. Aquaculture 39, 197–215. https://doi.org/10.1016/0044-8486(84)90266-7.
Hiong, K.C., Cao-Pham, A.H., Choo, C.Y., Boo, M.V., Wong, W.P., Chew, S.F., Ip, Y.K., 2017. Light-dependent expression of a na^+/h^+ exchanger 3-like transporter in the ctenidium of the giant clam, *tridacna squamosa*, can be related to increased h+ excretion during light-enhanced calcification. Phys. Rep. 5, e13209. https://doi.org/10.14814/phy2.13209.
Hori, M., Sano, Y., Ishida, A., Takahata, N., Shirai, K., Watanabe, T., 2015. Middle Holocene daily light cycle reconstructed from the strontium/calcium ratios of a fossil giant clam shell. Sci. Rep. 5, 1–5. https://doi.org/10.1038/srep08734.
Immenhauser, A., Schöne, B.R., Hoffmann, R., Niedermayr, A., 2016. Mollusc and brachiopod skeletal hard parts: intricate archives of their marine environment. Sedimentology 63, 1–59. https://doi.org/10.1111/sed.12231.
Ip, Y.K., Hiong, K.C., Goh, E.J., Boo, M.V., Choo, C.Y., Ching, B., Wong, W.P., Chew, S.F., 2017. The whitish inner mantle of the giant clam, *Tridacna squamosa*, expresses an apical plasma membrane Ca2+-ATPase (PMCA) which displays light-dependent gene and protein expressions. Front. Physiol. 8, 1–14. https://doi.org/10.3389/fphys.2017.00781.
Iponre, V., 2009. Vietnam Assessment Report on Climate Change (Varcc). Van hoa-Thong tin Publishing House, pp. 25–71.
Ishikura, M., Kato, C., Maruyama, T., 1997. UV-absorbing substances in zooxanthellate and azooxanthellate clams. Mar. Biol. 128, 649–655. https://doi.org/10.1007/s002270050131.
Janse, M., Wensing, J., Gieling, H., de Jongh, T., Leewis, R., 2008. Ecological management of a large coral reef eco-display at burgers' zoo, Arnhem, the Netherlands. In: Leewis, R.J., Janse, M. (Eds.), Advances in Coral Husbandry in Public Aquariums Public Aquarium Husbandry Series. Burgers' Zoo, Arnhem, pp. 293–303.
Jansen, E., Overpeck, J., Briffa, K., Duplessy, J.C., Joos, F., Masson-Delmotte, V., Olago, D., Otto-Bliesner, B., Peltier, W., Rahmstorf, S., Ramesh, R., Raynaud, D., Rind, D., Solomina, O., Villalba, R., Zhang, D., 2007. Palaeoclimate. In: Solomon, S., Qin, D., Manning, M., Chen, Z., Marquis, M., Averyt, K., Tignor, M., Miller, H. (Eds.), Climate Change 2007: The Physical Science Basis. Contribution of Working Group I to the Fourth Assessment Report of the Intergovernmental Panel on Climate Change. Cambridge University Press, Cambridge, United Kingdom and New York, NY, USA, pp. 433–497.
Jantzen, C., Wild, C., El-Zibdah, M., Roa-Quiaoit, H.A., Haacke, C., Richter, C., 2008. Photosynthetic performance of giant clams, *Tridacna maxima* and *T. squamosa,* Red Sea. Mar. Biol. 155, 211–221. https://doi.org/10.1007/s00227-008-1019-7.
Ji, X., Shu, L., Li, J., Zhao, C., Chen, W., Chen, Z., Shang, X., Dahlgren, R.A., Yang, Y., Zhang, M., 2022. Tracing nitrate sources and transformations using $\delta_{17}O$, $\delta_{15}N$, and $\delta_{18}O$ NO_3 in a coastal plain river network of eastern China. J. Hydrol. 610, 127829. https://doi.org/10.1016/j.jhydrol.2022.127829.
Jochum, K.P., Stoll, B., Herwig, K., Willbold, M., Hofmann, A.W., Amini, M., Aarburg, S., Abouchami, W., Hellebrand, E., Mocek, B., et al., 2006. Mpi-ding reference glasses for in situ microanalysis: new reference values for element concentrations and isotope ratios. Geochem. Geophys. Geosyst. 7. https://doi.org/10.1029/2005GC001060.
Jochum, K.P., Weis, U., Stoll, B., Kuzmin, D., Yang, Q., Raczek, I., Jacob, D.E., Stracke, A., Birbaum, K., Frick, D.A., Günther, D., Enzweiler, J., 2011. Determination of reference values for NIST SRM 610-617 glasses following ISO guidelines. Geostand. Geoanal. Res. 35, 397–429. https://doi.org/10.1111/j.1751-908X.2011.00120.x.
Johnson, A.L., Hickson, J.A., Bird, A., Schöne, B.R., Balson, P.S., Heaton, T.H., Williams, M., 2009. Comparative sclerochronology of modern and mid-Pliocene (c. 3.5 Ma) *Aequipecten opercularis* (Mollusca, Bivalvia): an insight into past and future climate change in the north-East Atlantic region. Palaeogeogr. Palaeoclimatol. Palaeoecol. 284, 164–179. https://doi.org/10.1016/j.palaeo.2009.09.022.
Jones, D.S., Quitmyer, I.R., 1996. Marking time with bivalve shells: oxygen isotopes and season of annual increment formation. Palaios 11, 340–346. https://doi.org/10.2307/3515244.
Jones, D.S., Williams, D.F., Arthur, M.A., 1983. Growth history and ecology of the Atlantic surf clam, *Spisula solidissima* (Dillwyn), as revealed by stable isotopes and annual shell increments. J. Exp. Mar. Biol. Ecol. 73, 225–242. https://doi.org/10.1016/0022-0981(83)90049-7.
Jones, D.S., Williams, D.F., Romanek, C.S., 1986. Life history of symbiont-bearing giant clams from stable isotope profiles. Science 231, 46–48. https://doi.org/10.1126/science.231.4733.46.
Jones, D.S., Arthur, M.A., Allard, D.J., 1989. Sclerochronological records of temperature and growth from shells of *Mercenaria mercenaria* from Narragansett Bay, Rhode Island. Mar. Biol. 102, 225–234. https://doi.org/10.1007/BF00428284.
Jones, D.S., Quitmyer, I.R., Andrus, C.F.T., 2005. Oxygen isotopic evidence for greater seasonality in Holocene shells of *Donax variabilis* from Florida. Palaeogeogr. Palaeoclimatol. Palaeoecol. 228, 96–108. https://doi.org/10.1016/j.palaeo.2005.03.046.
Jouzel, J., Koster, R.D., Suozzo, R.J., Russell, G.L., 1994. Stable water isotope behavior during the last glacial maximum: a general circulation model analysis. J. Geophys. Res. 99. https://doi.org/10.1029/94jd01819.
Keith, M.L., Anderson, G.M., Eichler, R., 1964. Carbon and oxygen isotopic composition of mollusk shells from marine and fresh-water environments. Geochim. Cosmochim. Acta 28, 1757–1786. https://doi.org/10.1016/0016-7037(64)90021-3.
Klein, R.T., Lohmann, K.C., Thayer, C.W., 1996. Sr/Ca and $_{13}C/_{12}C$ ratios in skeletal calcite of *Mytilus trossulus*: Covariation with metabolic rate, salinity, and carbon isotopic composition of seawater. Geochim. Cosmochim. Acta 60, 4207–4221. https://doi.org/10.1016/S0016-7037(96)00232-3.
Komagoe, T., Watanabe, T., Shirai, K., Yamazaki, A., Uematu, M., 2018. Geochemical and microstructural signals in giant clam *Tridacna maxima* recorded typhoon events at Okinotori Island, Japan. J. Geophys. Res. Biogeosci. 123, 1460–1474. https://doi.org/10.1029/2017JG004082.
Koop, K., Booth, D., Broadbent, A., Brodie, J., Bucher, D., Capone, D., Coll, J., Dennison, W., Erdmann, M., Harrison, P., Hoegh-Guldberg, O., Hutchings, P., Jones, G.B., Larkum, A.W., O'Neil, J., Steven, A., Tentori, E., Ward, S., Williamson, J., Yellowlees, D., 2001. ENCORE: the effect of nutrient enrichment on coral reefs. Synthesis of results and conclusions. Mar. Pollut. Bull. 42, 91–120. https://doi.org/10.1016/S0025-326X(00)00181-8.
Krants, D.E., J.D.S, Williams, D.F., 1984. Growth rates of the sea scallop, *Placopecten Magellanicus*, determined from the $_{18}O/_{16}O$ record in shell calcite. Biol. Bull. 167, 186–199. https://doi.org/10.2307/1541347.
Li, J., Volsteadt, M., Kirkendale, L., Cavanaugh, C.M., 2018. Characterizing photosymbiosis between fraginae bivalves and symbiodinium using phylogenetics and stable isotopes. Front. Ecol. Evol. 6, 1–11. https://doi.org/10.3389/fevo.2018.00045.
Liu, Y.W., Aciego, S.M., Wanamaker Jr., A.D., 2015. Environmental controls on the boron and strontium isotopic composition of aragonite shell material of cultured *Arctica islandica*. Biogeosciences 12 (11), 3351–3368. https://doi.org/10.5194/bg-12-3351-2015.
Liu, C., Li, X., Wu, C., Wang, A., Gu, Z., 2020. Effects of three light intensities on the survival, growth performance and biochemical composition of two size giant clams *Tridacna crocea* in the Southern China Sea. Aquaculture 528, 735548. https://doi.org/10.1016/j.aquaculture.2020.735548.
Liu, C., Zhao, L., Zhao, N., Yang, W., Hao, J., Qu, X., Liu, S., Dodson, J., Yan, H., 2022. Novel methods of resolving daily growth patterns in giant clam (*Tridacna spp.*) shells. Ecol. Indic. 134, 108480. https://doi.org/10.1016/j.ecolind.2021.108480.
Longerich, H.P., Jackson, S.E., Günther, D., 1996. Laser ablation inductively coupled plasma mass spectrometric transient signal data acquisition and analyte concentration calculation. J. Anal. At. Spectrom. 11, 899–904. https://doi.org/10.1039/JA9961100899.
Loo, S.E., Ryan, M.C., Zebarth, B.J., Kuchta, S.H., Neilsen, D., Mayer, B., 2017. Use of $\delta_{15}N$ and $\delta_{18}O$ values for nitrate source identification under irrigated crops: a

cautionary vadose zone tale. J. Environ. Qual. 46, 528–536. https://doi.org/10.2134/jeq2016.08.0294.
Lopes Dos Santos, R.A., Spooner, M.I., Barrows, T.T., De Deckker, P., Sinninghe Damsté, J.S., Schouten, S., 2013. Comparison of organic (UK'37, TEXH86, LDI) and faunal proxies (foraminiferal assemblages) for reconstruction of late Quaternary Sea surface temperature variability from offshore southeastern Australia. Paleoceanography 28, 377–387. https://doi.org/10.1002/palo.20035.
Lorens, R.B., Bender, M.L., 1980. The impact of solution chemistry on *Mytilus edulis* calcite and aragonite. Geochim. Cosmochim. Acta 44, 1265–1278. https://doi.org/10.1016/0016-7037(80)90087-3.
Lorrain, A., Paulet, Y.M., Chauvaud, L., Dunbar, R., Mucciarone, D., Fontugne, M., 2004. $\delta_{13}C$ variation in scallop shells: increasing metabolic carbon contribution with body size? Geochim. Cosmochim. Acta 68, 3509–3519. https://doi.org/10.1016/j.gca.2004.01.025.
Lucas, J.S., 1994. The biology, exploitation, and mariculture of giant clams (*Tridacnidae*). Rev. Fish. Sci. 2, 181–223. https://doi.org/10.1080/10641269409388557.
Ma, X., Yan, H., Fei, H., Liu, C., Shi, G., Huang, E., Wang, Y., Qu, X., Lian, E., Dang, H., 2020. A high-resolution δ18O record of modern *Tridacna gigas* bivalve and its paleoenvironmental implications. Palaeogeogr. Palaeoclimatol. Palaeoecol. 554, 109800. https://doi.org/10.1016/j.palaeo.2020.109800.
Maboloc, E.A., Puzon, J.J.M., Villanueva, R.D., 2015. Stress responses of zooxanthellae in juvenile *Tridacna gigas* (Bivalvia, Cardiidae) exposed to reduced salinity. Hydrobiologia 762, 103–112. https://doi.org/10.1007/s10750-015-2341-y.
Marshall, J.F., McCulloch, M.T., 2001. Evidence of El Niño and the Indian Ocean Dipole from Sr/Ca derived SSTs for modern corals at Christmas Island, Eastern Indian Ocean. Geophys. Res. Lett. 28, 3453–3456. https://doi.org/10.1029/2001GL012978.
McClelland, H.L., Halevy, I., Wolf-Gladrow, D.A., Evans, D., Bradley, A.S., 2021. Statistical uncertainty in paleoclimate proxy reconstructions. Geophys. Res. Lett. 48, 1–11. https://doi.org/10.1029/2021GL092773.
McConnaughey, T., 1989. 13c and 18o isotopic disequilibrium in biological carbonates: I. Patterns. Geochim. Cosmochim. Acta 53, 151–162. https://doi.org/10.1016/0016-7037(89)90282-2.
McConnaughey, T.A., Gillikin, D.P., 2008. Carbon isotopes in mollusk shell carbonates. Geo-Mar. Lett. 28, 287–299. https://doi.org/10.1007/s00367-008-0116-4.
Meibom, A., Farges, F., Stolarski, J., Dauphin, Y., Janoush, M., 2007. Speciation of Mg in biologically produced calcium carbonates. In: AGU Fall Meeting Abstracts. PP31C–0535.
Mezger, E., De Nooijer, L., Boer, W., Brummer, G., Reichart, G., 2016. Salinity controls on Na incorporation in red sea planktonic foraminifera. Paleoceanography 31, 1562–1582.
Mies, M., Braga, F., Scozzafave, M.S., de Lemos, D.E.L., Sumida, P.Y.G., 2012. Early development, survival and growth rates of the giant clam *Tridacna crocea (Bivalvia: Tridacnidae)*. Braz. J. Oceanogr. 60, 127–133. https://doi.org/10.1590/S1679-87592012000200003.
Mills, K., Sosdian, S., Muir, D., John, E., Nadia, S., Johnson, K., Buse, B., Waheed, Z., 2024. Giant Clams Modify Crystallographic and Geochemical Pathways of Shell Formation in Response to Turbidity. https://doi.org/10.21203/rs.3.rs-3832703/v1.
Muir, P.R., Sutton, D.C., Owens, L., 1991. Nitrate toxicity to *Penaeus monodon* protozoea. Mar. Biol. 108, 67–71. https://doi.org/10.1007/BF01313472.
Müller, W., Fietzke, J., 2016. The role of LA-ICP-MS in palaeoclimate research. Elements 12, 329–334. https://doi.org/10.2113/gselements.12.5.329.
Müller, W., Shelley, M., Miller, P., Broude, S., 2009. Initial performance metrics of a new custom-designed ArF excimer LA-ICPMS system coupled to a two-volume laser-ablation cell. J. Anal. At. Spectrom. 24, 209–214. https://doi.org/10.1039/b805995k.
Ngo-Duc, T., 2014. Climate change in the coastal regions of Vietnam. In: Coastal Disasters and Climate Change in Vietnam. Elsevier, pp. 175–198. https://doi.org/10.1016/B978-0-12-800007-6.00008-3 chapter 8.
Owen, R.A., Day, C.C., Hu, C.Y., Liu, Y.H., Pointing, M.D., Blättler, C.L., Henderson, G. M., 2016. Calcium isotopes in caves as a proxy for aridity: modern calibration and application to the 8.2 kyr event. Earth Planet. Sci. Lett. 443, 129–138. https://doi.org/10.1016/j.epsl.2016.03.027.
Paton, C., Hellstrom, J., Paul, B., Woodhead, J., Hergt, J., 2011. Iolite: Freeware for the visualisation and processing of mass spectrometric data. J. Anal. At. Spectrom. 26, 2508–2518. https://doi.org/10.1039/c1ja10172b.
Pätzold, J., Heinrichs, J.P., Wolschendorf, K., Wefer, G., 1991. Correlation of stable oxygen isotope temperature record with light attenuation profiles in reef-dwelling Tridacna shells. Coral Reefs 10, 65–69. https://doi.org/10.1007/BF00571825.
Pérez-Huerta, A., Etayo-Cadavid, M.F., Andrus, C.F.T., Jeffries, T.E., Watkins, C., Street, S.C., Sandweiss, D.H., 2013. El Niño impact on Mollusk biomineralization-implications for trace element proxy reconstructions and the paleo-archeological record. PLoS One 8. https://doi.org/10.1371/journal.pone.0054274.
Poulain, C., Gillikin, D., Thébault, J., Munaron, J., Bohn, M., Robert, R., Paulet, Y.M., Lorrain, A., 2015. An evaluation of Mg/Ca, Sr/Ca and Ba/Ca ratios as environmental proxies in aragonite bivalve shells. Chem. Geol. 396, 42–50. https://doi.org/10.1016/j.chemgeo.2014.12.019.
Prendergast, A.L., Versteegh, E.A., Schöne, B.R., 2017. New research on the development of high-resolution palaeoenvironmental proxies from geochemical properties of biogenic carbonates. Palaeogeogr. Palaeoclimatol. Palaeoecol. 484, 1–6. https://doi.org/10.1016/j.palaeo.2017.05.032.
Purton, L.M., Shields, G.A., Brasier, M.D., Grime, G.W., 1999. Metabolism controls Sr/Ca ratios in fossil aragonitic mollusks. Geology 27, 1083–1086. https://doi.org/10.1130/0091-7613(1999)027<1083:MCSCRI>2.3.CO;2.
Rebetez, M., Dupont, O., Giroud, M., 2009. An analysis of the July 2006 heatwave extent in Europe compared to the record year of 2003. Theor. Appl. Climatol. 95, 1–7. https://doi.org/10.1007/s00704-007-0370-9.
Romanek, C.S., Grossman, E.L., 1989. Stable isotope profiles of *tridacna maxima* as environmental indicators. Palaios 402–413. https://doi.org/10.2307/3514585.
Romanek, C.S., Jones, D.S., Williams, D.F., Krantz, D.E., Radtke, R., 1987. Stable isotopic investigation of physiological and environmental changes recorded in shell carbonate from the giant clam *Tridacna maxima*. Mar. Biol. 94, 385–393. https://doi.org/10.1007/BF00428244.
Rosewater, J., 1965. The family *tridacnidae* in the indo-pacific. Indo-Pacific Mollusca 1, 347.
Rossi, F., Herman, P., Middelburg, J., 2004. Interspecific and intraspecific variation of δc and δn in deposit-and suspension-feeding bivalves (*macoma balthica* and *cerastoderma edule*): evidence of ontogenetic changes in feeding mode of *macoma balthica*. Limnol. Oceanogr. 49, 408–414.
Sano, Y., Kobayashi, S., Shirai, K., Takahata, N., Matsumoto, K., Watanabe, T., Sowa, K., Iwai, K., 2012. Past daily light cycle recorded in the strontium/calcium ratios of giant clam shells. Nat. Commun. 3. https://doi.org/10.1038/ncomms1763.
Sano, Y., Okumura, T., Murakami-Sugihara, N., Tanaka, K., Kagoshima, T., Ishida, A., Hori, M., Snyder, G.T., Takahata, N., Shirai, K., 2021. Influence of normal tide and the Great Tsunami as recorded through hourly-resolution micro-analysis of a mussel shell. Nat. Sci. Rep. 1, 19874. https://doi.org/10.1038/s41598-021-99361-2.
Sanyal, A., Nugent, M., Reeder, R.J., Bijma, J., 2000. Seawater pH control on the boron isotopic composition of calcite: evidence from inorganic calcite precipitation experiments. Geochim. Cosmochim. Acta 64, 1551–1555. https://doi.org/10.1016/S0016-7037(99)00437-8.
Scaife, A., Knight, J., 2008. Ensemble simulations of the cold european winter of 2005-2006. Q. J. R. Meteorol. Soc. 134, 1647–1659.
Schleinkofer, N., Raddatz, J., Evans, D., Gerdes, A., Flögel, S., Voigt, S., Büscher, J.V., Wisshak, M., 2021. Compositional variability of Mg/Ca, Sr/Ca, and Na/Ca in the deep-sea bivalve *Acesta excavata* (Fabricius, 1779). PLoS One 16, 1–24. https://doi.org/10.1371/journal.pone.0245605.
Schlöder, C., D'Croz, L., 2004. Responses of massive and branching coral species to the combined effects of water temperature and nitrate enrichment. J. Exp. Mar. Biol. Ecol. 313, 255–268. https://doi.org/10.1016/j.jembe.2004.08.012.
Schöne, B.R., Fiebig, J., 2009. Seasonality in the North Sea during the Allerød and late medieval climate optimum using bivalve sclerochronology. Int. J. Earth Sci. 98, 83–98. https://doi.org/10.1007/s00531-008-0363-7.
Schöne, B.R., Gillikin, D.P., 2013. Unraveling environmental histories from skeletal diaries - advances in sclerochronology. Palaeogeogr. Palaeoclimatol. Palaeoecol. 373, 1–5. https://doi.org/10.1016/j.palaeo.2012.11.026.
Schöne, B.R., Lega, J., Flessa, K.W., Goodwin, D.H., Dettman, D.L., 2002. Reconstructing daily temperatures from growth rates of the intertidal bivalve mollusk Chione cortezi (northern Gulf of California, Mexico). Palaeogeogr. Palaeoclimatol. Palaeoecol. 184, 131–146. https://doi.org/10.1016/S0031-0182(02)00252-3.
Schöne, B.R., Houk, S.D., Freyre Castro, A.D., Fiebig, J., Oschmann, W., Kröncke, I., Dreyer, W., Gosselck, F., 2005. Daily growth rates in shells of *Arctica islandica*: assessing sub-seasonal environmental controls on a long-lived bivalve mollusk. Palaios 20, 78–92. https://doi.org/10.2110/palo.2003.p03-101.
Selin, N.I., Latypov, Y.Y., 2011. The size and age structure of *Tridacna crocea* Lamarck, 1819 (*Bivalvia: Tridacnidae*) in the coastal area of islands of the Cön Dao Archipelago in the South China Sea. Russ. J. Mar. Biol. 37, 376–383. https://doi.org/10.1134/S1063074011050129.
Sinclair, D.J., Kinsley, L.P., Mcculloch, M.T., 1998. High resolution analysis of trace elements in corals by laser ablation ICP-MS. Geochim. Cosmochim. Acta 62, 1889–1901. https://doi.org/10.1016/S0016-7037(98)00112-4.
Smith, S.V., Buddemeier, R.W., Redalje, R.C., Houck, J.E., 1979. Strontium-calcium thermometry in coral skeletons. Science 204, 404–407. https://doi.org/10.1126/science.204.4391.404.
Spötl, C., Vennemann, T.W., 2003. Continuous-flow isotope ratio mass spectrometric analysis of carbonate minerals. Rapid Commun. Mass Spectrom. 17, 1004–1006. https://doi.org/10.1002/rcm.1010.
Stecher, H.A., Krantz, D.E., Lord, C.J., Luther, G.W., Bock, K.W., 1996. Profiles of strontium and barium in *Mercenaria mercenaria* and *Spisula solidissima* shells. Geochim. Cosmochim. Acta 60, 3445–3456. https://doi.org/10.1016/0016-7037(96)00179-2.
Strasser, C.A., Mullineaux, L.S., Walther, B.D., 2008. Growth rate and age effects on *Mya arenaria* shell chemistry: implications for biogeochemical studies. J. Exp. Mar. Biol. Ecol. 355, 153–163. https://doi.org/10.1016/j.jembe.2007.12.022.
Surge, D., Walker, K.J., 2006. Geochemical variation in microstructural shell layers of the southern quahog (*Mercenaria campechiensis*): implications for reconstructing seasonality. Palaeogeogr. Palaeoclimatol. Palaeoecol. 237, 182–190. https://doi.org/10.1016/j.palaeo.2005.11.016.
Takesue, R.K., van Geen, A., 2004. Mg/Ca, Sr/Ca, and stable isotopes in modern and Holocene *Protothaca staminea* shells from a northern California coastal upwelling region. Geochim. Cosmochim. Acta 68, 3845–3861. https://doi.org/10.1016/j.gca.2004.03.021.
Tal, Y., Nussinovitch, A., Van Rijn, J., 2003. Nitrate removal in aquariums by immobilized Pseudomonas. Biotechnol. Prog. 19, 1019–1021. https://doi.org/10.1021/bp0200088.
Trinidad-Roa, M., 1988. Spawning and Larval Rearing of Giant Clams in Pangasinan, Philippines.
Ungvari, Z., Csiszar, A., Sosnowska, D., Philipp, E.E., Campbell, C.M., McQuary, P.R., Chow, T.T., Coelho, M., Didier, E.S., Gelino, S., Holmbeck, M.A., Kim, I., Levy, E., Sonntag, W.E., Whitby, P.W., Austad, S.N., Ridgway, I., 2013. Testing predictions of the oxidative stress hypothesis of aging using a novel invertebrate model of

longevity: the giant clam (*Tridacna derasa*). J. Gerontol. A Biol. Sci. Med. Sci. 68, 359–367. https://doi.org/10.1093/gerona/gls159.

Vieten, R., Hernandez, F., 2021. Stalgrowth—a program to estimate speleothem growth rates and seasonal growth variations. Geosciences (Switzerland) 11, 25–29. https://doi.org/10.3390/geosciences11050187.

Warter, V., Müller, W., Wesselingh, F.P., Todd, J.A., Renema, W., 2015. Late Miocene seasonal to subdecadal climate variability in the Indo-west Pacific (East Kalimantan, Indonesia) preserved in giant clams. Palaios 30, 66–82. https://doi.org/10.2110/palo.2013.061.

Warter, V., Erez, J., Müller, W., 2018. Environmental and physiological controls on daily trace element incorporation in Tridacna crocea from combined laboratory culturing and ultra-high resolution LA-ICP-MS analysis. Palaeogeogr. Palaeoclimatol. Palaeoecol. 496, 32–47. https://doi.org/10.1016/j.palaeo.2017.12.038.

Watanabe, T., Oba, T., 1999. Daily reconstruction of water temperature from oxygen isotopic ratios of a modern Tridacna shell using a freezing microtome sampling technique. J. Geophys. Res. Oceans 104, 20667–20674. https://doi.org/10.1029/1999jc900097.

Watanabe, T., Suzuki, A., Kawahata, H., Kan, H., Ogawa, S., 2004. A 60-year isotopic record from a mid-Holocene fossil giant clam (*Tridacna gigas*) in the Ryukyu Islands: physiological and paleoclimatic implications. Palaeogeogr. Palaeoclimatol. Palaeoecol. 212, 343–354. https://doi.org/10.1016/j.palaeo.2004.07.001.

Wei, G., Sun, M., Li, X., Nie, B., 2000. Mg/Ca, Sr/Ca and U/Ca ratios of a porites coral from Sanya Bay, Hainan Island, South China Sea and their relationships to sea surface temperature. Palaeogeogr. Palaeoclimatol. Palaeoecol. 162, 59–74. https://doi.org/10.1016/S0031-0182(00)00105-X.

Weidman, C.R., Jones, G.A., Kyger, 1994. The long-lived mollusc *Arctica islandica*: a new paleoceanographic tool for the reconstruction of bottom temperatures for the continental shelves of the northern North Atlantic Ocean. J. Geophys. Res. 99, 305–314. https://doi.org/10.1029/94jc01882.

Welsh, K., Elliot, M., Tudhope, A., Ayling, B., Chappell, J., 2011. Giant bivalves (*Tridacna gigas*) as recorders of ENSO variability. Earth Planet. Sci. Lett. 307, 266–270. https://doi.org/10.1016/j.epsl.2011.05.032.

Yamanashi, J., Takayanagi, H., Isaji, A., Asami, R., Iryu, Y., 2016. Carbon and oxygen isotope records from *tridacna derasa* shells: toward establishing a reliable proxy for sea surface environments. PLoS One 11. https://doi.org/10.1371/journal.pone.0157659.

Yan, H., Shao, D., Wang, Y., Sun, L., 2013. Sr/Ca profile of long-lived *Tridacna gigas* bivalves from South China Sea: a new high-resolution SST proxy. Geochim. Cosmochim. Acta 112, 52–65. https://doi.org/10.1016/j.gca.2013.03.007.

Yan, H., Shao, D., Wang, Y., Sun, L., 2014. Sr/Ca differences within and among three Tridacnidae species from the South China Sea: implication for paleoclimate reconstruction. Chem. Geol. 390, 22–31. https://doi.org/10.1016/j.chemgeo.2014.10.011.

Yan, H., Sun, L., Shao, D., Wang, Y., 2015. Seawater temperature seasonality in the South China Sea during the late Holocene derived from high-resolution Sr/Ca ratios of Tridacna gigas. Quat. Res. (United States) 83, 298–306. https://doi.org/10.1016/j.yqres.2014.12.001.

Yan, H., Liu, C., An, Z., Yang, W., Yang, Y., Huang, P., Qiu, S., Zhou, P., Zhao, N., Fei, H., Ma, X., Shi, G., Dodson, J., Hao, J., Yu, K., Wei, G., Yang, Y., Jin, Z., Zhou, W., 2020. Extreme weather events recorded by daily to hourly resolution biogeochemical proxies of marine giant clam shells. Proc. Natl. Acad. Sci. USA 117, 7038–7043. https://doi.org/10.1073/pnas.1916784117.

Yang, Z., Shao, D., Mei, Y., Yang, W., Wang, Y., Sun, L., Xie, Z., 2019. The controlling mechanism of mid- to late Holocene carbon isotopic variations of *Tridacnidae* in the South China Sea. Mar. Geol. 415, 105958. https://doi.org/10.1016/j.margeo.2019.06.003.

Yu, J., Foster, G.L., Elderfield, H., Broecker, W.S., Clark, E., 2010. An evaluation of benthic foraminiferal B/Ca and δ_{11}B for deep ocean carbonate ion and pH reconstructions. Earth Planet. Sci. Lett. 293, 114–120. https://doi.org/10.1016/j.epsl.2010.02.029.

Zhao, N., Yan, H., Luo, F., Yang, Y., Liu, S., Zhou, P., Liu, C., Dodson, J., 2023. Daily growth rate variation in Tridacna shells as a record of tropical cyclones in the South China Sea: palaeoecological implications. Palaeogeogr. Palaeoclimatol. Palaeoecol. 615, 111444. https://doi.org/10.1016/j.palaeo.2023.111444.

Zhou, Z., Liu, Z., Wang, L., Luo, J., Li, H., 2019. Oxidative stress, apoptosis activation and symbiosis disruption in giant clam *Tridacna crocea* under high temperature. Fish Shellfish Immunol. 84, 451–457. https://doi.org/10.1016/j.fsi.2018.10.033.

Zhou, P., Yan, H., Shi, G., Liu, C., Luo, F., Han, T., Wang, G., Wen, H., Zhao, N., Dodson, J., Li, Y., Zhou, W., 2022. Sea surface temperature seasonality in the northern South China Sea during the middle Holocene derived from high resolution Sr/Ca ratios of Tridacna shells. Quat. Res. (United States) 105, 37–48. https://doi.org/10.1017/qua.2021.28.